

RAM

● ROBOTICS
AND
MECHATRONICS

USING MIXED-REALITY IN BIOPSY OF LESIONS INSIDE DEFORMABLE ORGANS

J.L. (Joost) van Smoorenburg

MSC ASSIGNMENT

Committee:

prof. dr. ir. S. Stramigioli
dr. V. Groenhuis, MSc
dr. F.J. Siepel, MSc
dr. ir. D. Reidsma

July 2021

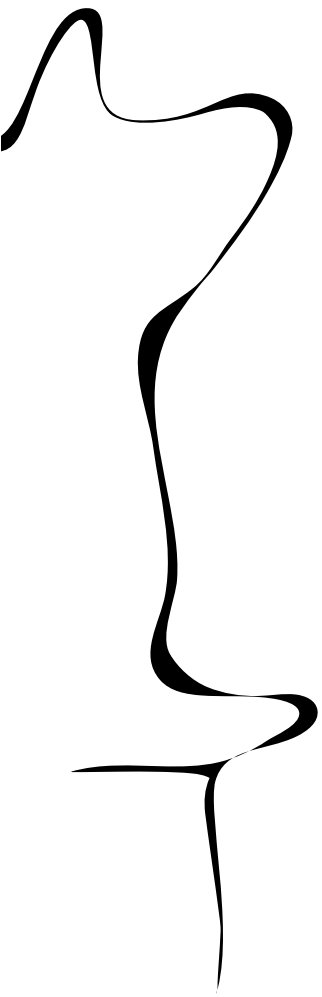
043RaM2021
Robotics and Mechatronics
EEMathCS
University of Twente
P.O. Box 217
7500 AE Enschede
The Netherlands

UNIVERSITY
OF TWENTE.

TECHMED
CENTRE

UNIVERSITY
OF TWENTE.

DIGITAL SOCIETY
INSTITUTE



Abstract

Breast screening is done to determine whether lesions are present in the breast. The biopsy of found lesions is usually done under the guidance of Ultrasound (US) to track the location of the needle in the breast. Some cancer types cannot be detected using US. Therefore, Magnetic Resonance Imaging (MRI) will instead be used for these types of cancer. An MR image gives a highly detailed image of the breast and enables visualization of most cancer types. A major disadvantage of using MRI for guided biopsies is the lack of real time information, since metal objects and electronics cannot go near the scanner once it is turned on due to the magnetic field this machine produces.

This work describes the implementation of a Mixed Reality guidance system to aid the surgeon when performing an MRI-guided biopsy. The proposed solution consists of 3 components. Measurements were performed using an Optitrack camera system which tracked retro reflective markers in 3D space. Matlab was used as the processing software and filtered and matched the measured marker data to the relevant objects and updated the position and shape of the hologram accordingly. The Thin Plate Spline algorithm was used to track deformations of the breast that could occur during the biopsy and updated the hologram to account for the change of position of the lesion. The Microsoft HoloLens was used to visualize the holograms of the breast which has been created from MRI data and placed them at the correct position in 3D space.

The solution is capable of placing the hologram with an error (E) of $(E_x, E_y, E_z) = (7.2, 9.6, 8.1)$ mm. 72 biopsies have been performed in this work, resulting in a 64% success rate when TPS was disabled and a 28% success rate when TPS was enabled. By combining those outcomes, a total success rate of 46% was achieved for the current implementation. Despite the final solution not surpassing the success rate of current MRI-guided biopsy techniques, further research in the area of using Mixed Reality for medical purposes could lead to state of the art products that will aid medical specialists in performing biopsies with more accuracy.

Contents

1	Introduction	1
1.1	Motivation	1
1.2	Background & Related work	3
1.2.1	Mixed Reality	3
1.2.2	HoloLens	3
1.2.3	Clinical procedures using Mixed Reality	4
1.3	Objective	5
1.4	Document overview	5
2	Method	6
2.1	Optitrack	6
2.1.1	Trackable objects	6
2.1.2	Hardware	9
2.1.3	Software	9
2.2	Matlab	10
2.2.1	Communication with Optitrack	11
2.2.2	Communication with HoloLens	11
2.2.3	Homogeneous matrix	11
2.2.4	Marker identification	12
2.2.5	Thin Plate Spline (TPS)	14
2.2.6	Graphical User Interface (GUI)	14
2.3	Unity	15
2.4	Experiments	17
2.4.1	Hologram placement error evaluation	17
2.4.2	Marker filtering	18
2.4.3	Thin Plate Spline validation	18
2.4.4	Biopsy	18
3	Results	20
3.1	Hologram placement	20
3.2	Marker filtering	22
3.3	Thin Plate Spline (TPS) validation	23
3.4	Biopsy	25
4	Discussion	27
4.1	Hologram placement error evaluation	27
4.2	Marker filtering	28
4.3	Thin Plate Spline (TPS)	28
4.4	Biopsy	28
5	Conclusion & Future work	31
5.1	Future work	31
6	Appendix A: Homogeneous matrices	33
6.1	Overview of frames	33
6.2	Static transformations	33
6.3	Chained multiplications	33

Acronyms

- AR** Augmented Reality. 2–4
- CPU** Central Processing Unit. 31
- CT** Computed Tomography. 4
- FoV** Field of View. 4, 9, 31
- GUI** Graphical User Interface. iii, 14, 15
- HMD** Head Mounted Device. 2–4, 17, 27, 28
- HPU** Holographic Processing Unit. 3
- IGS** Image Guided Surgery. 4
- IR** Infrared. 4
- LCNB** Large Core Needle Biopsy. 2
- MRI** Magnetic Resonance Imaging. ii, 1–5, 7, 8, 14, 30–32
- MTU** Maximum Transmission Unit. 11
- MxR** Mixed Reality. ii, 2–6, 15, 28, 31
- PLA** Polylactic Acid. 6
- RAM** Random Access Memory. 3, 31
- RMS** Root Mean Square. 13
- STL** Standard Triangle Language. 15
- TPS** Thin Plate Spline. ii, iii, 10, 14, 15, 18, 20, 23–29, 31, 32
- US** Ultrasound. 1
- USB** Universal Serial Bus. 3, 9, 17
- VAB** Vacuum Assisted Biopsy. 2
- VC** Virtuality Continuum. 3
- VR** Virtual Reality. 3
- WDP** Windows Device Portal. 17

1 Introduction

1.1 Motivation

Breast cancer is the most common cancer diagnosed among American women (excluding skin cancers) and is the second leading cause of cancer death among women after lung cancer[15]. It is estimated that 1 out of 8 American woman will get breast cancer [5]. Early detection and treatment of cancerous cells in the breast will drastically increase the rate of survival, with the 5 year relative survival rate of localized breast cancer being 99% [11]. Breast screening is done to determine whether lesions are present in the breast. Whenever a lesion has been detected, a biopsy is performed to evaluate the nature of the lesion. This is essential to determine if a lesion is malicious and what type of treatment should be applied.

Different screening methods can be used to determine the presence and position of a lesion, namely Mammography, Ultrasound (US) & Magnetic Resonance Imaging (MRI). Mammography is the first step in breast screening, which uses low energy x-rays to scan the breast tissue for irregularities. The breast is compressed between two plates to even out the tissue and the resulting image is analyzed by a radiologist for characteristic masses.

If suspicious lesions have been found, the doctor might use US to acquire more detailed information from the tissue surrounding the lesion. US uses high frequency sound waves to visualize breast tissue. By using a handheld US probe, the doctor can scan and visualize a region of interest. Scanning the tissue surrounding the lesion might give the doctor enough insights to classify whether a lesion is malicious or benign.

If the lesion cannot be classified correctly using the previously mentioned techniques, the doctor will turn to Magnetic Resonance Imaging. MRI is a technique that uses a magnetic field to create images of organic material. Hydrogen atoms are used to generate a polarization that can be detected by the antenna which is present in the machine [19]. MRI creates high quality images on which lesions can be detected which cannot be seen using US or Mammography [25]. However, a downside of the technique is that it is quite expensive and time consuming. Before the MRI-scan, the patient is injected with a contrast agent. Cancerous lesions tend to display abnormal vessels that are "leaky" compared to the vessels of normal structures. This allows the contrast agent to pool in the interstitial spaces, thereby making them visible on MRI [42]. An example of the effect of the contrast agent is shown in figure 1.

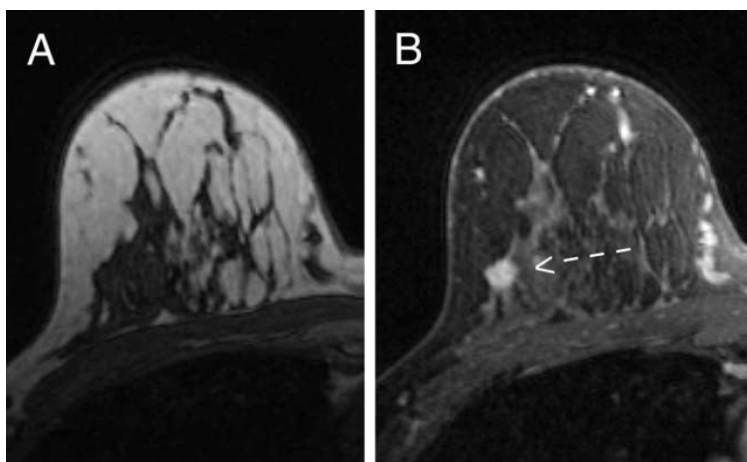


Figure 1: Comparison of MRI results without (A) and with (B) contrast agent. The arrow indicates the position of the tumor. Source: [42].

Before the doctor can give a final verdict about the nature of the lesion, part of the lesion tissue should be extracted by means of biopsy. This is done by placing a needle in the breast at the position of the lesion and extracting some tissue so that its structure can be further investigated in the lab. Positioning the biopsy needle at the right place is a challenging operation since the doctor cannot place the needle accurately into the breast without visual aid. This may require multiple biopsies to be performed before accurately reaching the lesion. Since performing a biopsy causes major discomfort for the patient, the operation should, desirably, only be performed once. Image guided biopsy is a helpful tool to solve this problem. US-guided biopsy is the preferred method for image guided biopsy as it is less invasive, less expensive and less time consuming than surgical biopsy [36]. Nevertheless, some lesions might not be visible using US. In these cases an MRI-guided

biopsy is performed. The main problem with this technique is that there is no space in the MRI machine to reach the patient to perform the biopsy when the patient is in the scanner. Another problem is that an MRI machine uses big magnets to create the magnetic field that is needed to acquire the image. Metal objects, like needles or wires, cannot be near the scanner once it is turned on. Patients will have to be removed out of the machine and transported to another room before the biopsy can be performed. This might introduce a change of pose of the patient and thus a position change of the lesion.

in MRI-guided biopsies, rosters are usually used to accurately place the needle in the breast. Based on the MR image, the correct roster hole is calculated to allow for the needle to reach the lesion of interest. An schematic of such system is shown in figure 2. Meeuwis et al. [27] investigated the success rates when using two MRI-guided biopsy techniques, the Large Core Needle Biopsy (LCNB) biopsy and Vacuum Assisted Biopsy (VAB) biopsy. They have achieved success rates of 100% for the LCNB and 98% for the VAB technique, which translates to a single failed biopsy using VAB. Imschweiler et al. [20] performed 557 MRI-guided VAB and had a success rate of 98.4%. The results insinuate that these techniques show great results when extracting tissue from a calculated position in the breast.

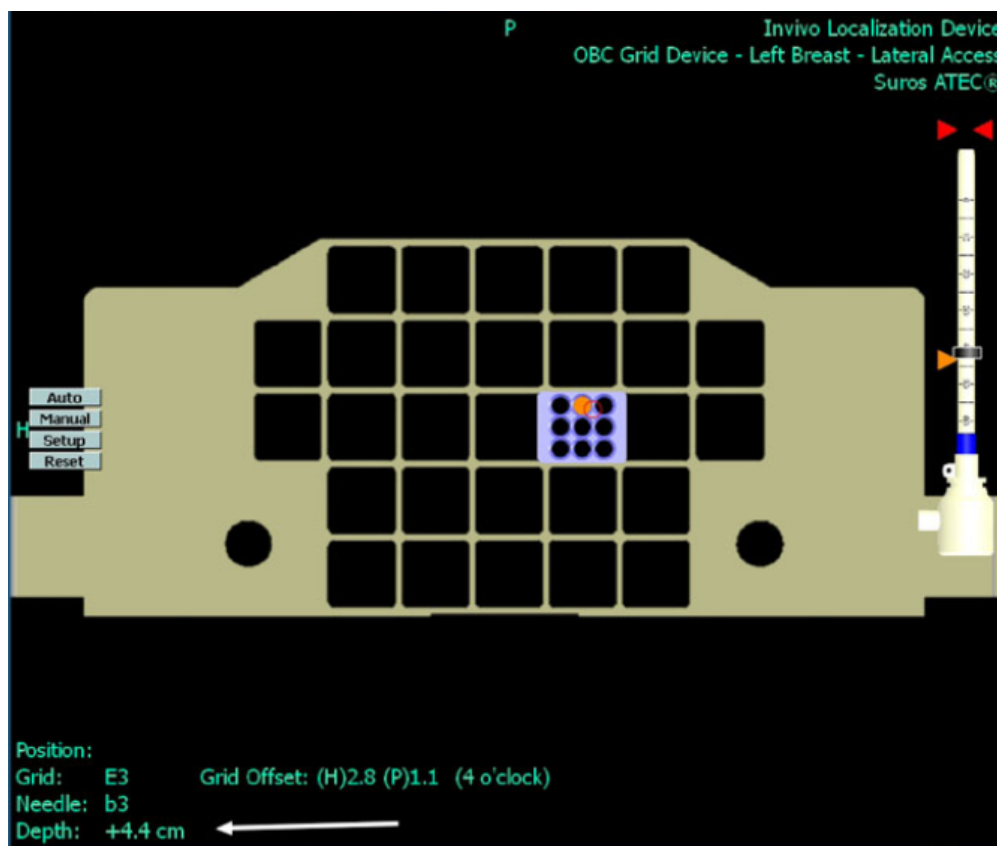


Figure 2: A visualization of the system used for VAB, the correct position for the grid, needle and depth have been calculated using the MRI image and are shown in the bottom left. The actual position of the lesion is marked with a red circle close to the orange dot. Source:[27]

A downside of previously mentioned techniques is that the needle can only be inserted in a restricted angular range and that the lesion can only be targeted from the outside of the breast, meaning that the entire breast has to be perforated to reach the potential malignant lump. This will introduce more pain for the patient since deep lesions are more painful than superficial ones. [18]. This can also be seen when looking closely at figure 2. The orange circle, which marks the most optimal place for the needle, does not align well with the red circle, which is the actual position of the lesion. Another approach to perform the biopsy is by means of a robot. Groenhuis et al. [17] have created multiple iterations of a robot which can be placed in the MRI scanner since it is created from MR safe materials only. The robot is controlled pneumatically which eliminates the need for copper wires.

This work will investigate the usability of using Mixed Reality (MxR) to aid doctors in accurately performing a biopsy. MxR, sometimes referred to as Augmented Reality (AR), requires the user to wear a Head Mounted Device (HMD) to project digital 3D content on a see through display by means of holograms.

These holograms can be placed relative to real life objects since the HMD has spatial awareness and can detect structures and its position relative to those structures.

By visualizing holograms of lesions, acquired from MR-images, and precisely positioning those holograms over the actual breast, a biopsy could possibly be performed more accurately than without this visual aid. To track the breast, retroreflective markers will be placed on the breast during the MRI scan to enable automatic alignment of the hologram on top of the breast by tracking the markers with a camera setup. These markers can also be used to track deformations of the breast that might occur when the needle is inserted into it, computer models can calculate the change of the position of the lesion and can update the hologram accordingly.

1.2 Background & Related work

1.2.1 Mixed Reality

Mixed Reality (MxR) is a description used to describe the merging of both virtual and real environments. Figure 3 shows the position of MxR on the Virtuality Continuum (VC), which is a scale that describes the realness of objects from completely virtual to completely real. MxR was first mentioned in [29], in which the need for taxonomy of the technology was described to create structural classes to which meaningfully data comparison and discussions can be made. Since MxR is present in nearly all of the VC, distinctions need to be made with other realities present in the scale.

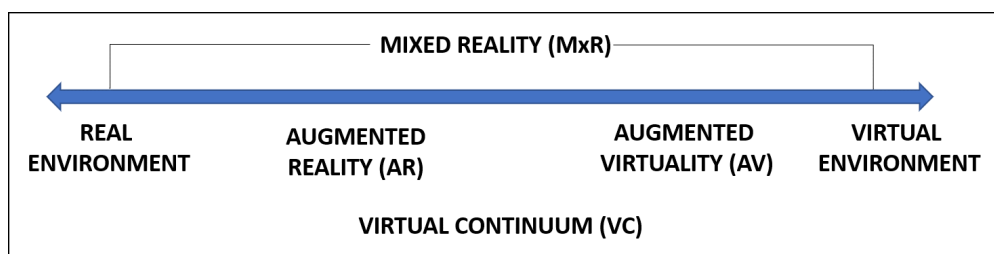


Figure 3: Simplified representation of a "virtuality continuum". Image recreated using [29].

Virtual Reality (VR) creates a complete virtual world in which the user is totally immersed. This world can be created to include anything the creator can think of and does not have to be linked to the real world. The VR can be entered using a suitable HMD like the Oculus Rift (Facebook, Inc., Menlo Park, CA, USA) or HTC Vive (HTC, Xindian, New Taipei, Taiwan). The main difference compared to MxR is that VR places the subject in a complete virtual world without interaction with the real environment, while MxR projects virtual content in 3D objects in the real environment.

Another position on the VC is AR, which adds digital objects to a live view which can help to visualize new products in existing environments like spatial planning in road working. Rokhsaritalemi et al. [35] stated that the only main difference between MxR and AR is the awareness feature, in which MxR has perfectly rendered virtual objects that cannot be distinguished from real objects and AR has virtual objects that can be identified based on their nature and behavior like floating text that follows a user. So it could be said that the main difference of MxR compared to AR is that in MxR the displayed digital information is not just an overlay, like in AR, but is actually placed in a 3D space and the user can walk around it to look at the projected information from different angles.

1.2.2 HoloLens

The Microsoft HoloLens (Microsoft, Redmond, WA, USA) is a HMD which is capable of visualizing MxR. The sensors which are present in the device are shown in table 1.

The HoloLens includes 2 processors to compute all necessary actions, the gestures and hologram projections are being handled by the custom build Holographic Processing Unit (HPU) and the regular computations are handled by the Intel Cherry Trail 32-bit processor. The device houses 2GB of RAM, 1GB for each processor, and has 64GB of internal storage. Communication with the device can be established via Wi-Fi, Bluetooth or via USB using the micro USB 2.0 port [4].

The device can be used together with the developed Mixed Reality Toolkit [3] to create MxR applications using the game engine Unity [6].

Sensor type	Count
Inertial Measurement Unit (IMU)	1
Environment understanding camera	4
Depth camera	1
RGB camera	1
Mixed Reality capture	1
Microphone	4
Ambient light sensor	1

Table 1: List of available sensors in the Microsoft HoloLens (1st gen). Source: [2].

The components of the HoloLens have been reviewed by different researchers, Kress and Cummings [22] have written down the technical details regarding the optical architecture of the device. Sharp et al. [37] have incorporated the advanced hand tracking mechanism used to control the HoloLens based on articulated hand tracking. Meulstee et al. [28] have created a setup to determine the accuracy of the HoloLens when used during Image Guided Surgery (IGS). The accuracy was tracked using reflective markers. Their main focus was to determine the influence of the HoloLens on the switching focus problem, which describes the switch of the view of the surgeon when he or she has to look away from the patient to a screen to get certain information. The results noted a mean Euclidean distance of 2.3 mm with a maximum error of 3.5 mm for the complete system when placing a hologram based on the position of the reflective markers. Vassallo et al. [40] have researched the stability of hologram placement without markers and came to an average error of 6 mm. Liu et al. [26] have investigated the accuracy in head localization, real environment reconstruction, spatial mapping and hologram placing using Infrared (IR) markers and an Optitrack system. They found an average position error of the HoloLens head localization feature of 5.3 mm when moving slowly and 16.3 mm when moving quickly respectively. Garon et al. [16] compared the acquired data from the depth sensor of the HoloLens with the data acquired from an external depth sensor and combined both to recreate high detail depth information of the FoV of the HoloLens.

1.2.3 Clinical procedures using Mixed Reality

Studies to research the influence of Mixed Reality in the operating room have been conducted. Some relevant studies will be described below.

Norberg et al. [30] used the HoloLens to visualize the outcome of breast reconstruction to give patients a better insight of the final result. Tepper et al. [38] described the use of the HoloLens to improve pre-operative planning or intraoperative navigation. Velazco-Garcia et al. [41] described the use of their FI3D cross-platform framework to visualize cardiac MRI data using the HMD as an output device and a dedicated server for computational demanding processes. Perkins et al. [32] used Mixed Reality to project the location of a palpable tumors in breast of woman in operative (supine) position. The authors used ArUco tags [1] on patients to align the hologram created from the MRI data correctly. They measured an mean error of -1 mm in the up-down dimension and -0.2 in the left-right dimension when comparing the actual tumour position with the position that was drawn by a surgeon based on the projected position of the lesion by means of a hologram. Kunz et al. [23] used the HoloLens and infrared markers to track the position of the skull and project a hologram with an accuracy of 0.76 mm during neurosurgical interventions. This solution does need a IR light source to light up the markers so that they can be detected by the cameras present on the HoloLens which has to be attached to the HoloLens or placed in the same room. Bettati et al. [13] used the HoloLens to create holograms of soft tissue and lung lesions using Computed Tomography (CT). They showed that including an AR model reduced the mean distance to the tumour center from 15.2 mm to 7.5 mm when performing biopsy on soft tissue lesions. Park et al. [31] used the HoloLens to research performance difference when performing biopsy on a phantom using participants with different levels of skill. Results show that the implementation of a hologram reduced the number of passes needed to reach the selected target from 7.4 to 3.4.

1.3 Objective

The objective of this work is to implement a solution that can generate a hologram of a breast and the lesion(s) inside of it to solve the lack of visual aid when performing a MRI-guided biopsy. A phantom will be used to simulate an actual breast. The hologram will be placed on top of the phantom by using the real-time 3D marker data acquired by the Optitrack Camera system. A Matlab program will process this data, update the meshes which describe the breast to account for any deformations and send the updated data to the HoloLens to be visualized at the correct position in 3D space. A visual overview of the proposed procedure is given in figure 4.

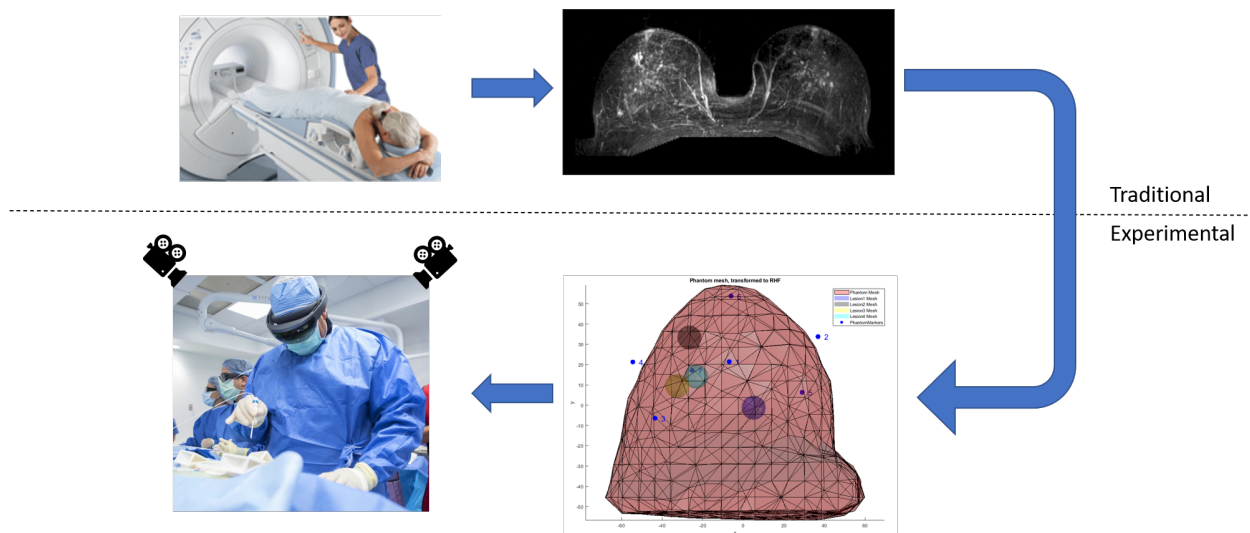


Figure 4: Proposed procedure overview. Taking an MRI-scan, determining the position of the lesion, creating the hologram, and finally performing biopsy using the HoloLens to visualize the hologram and cameras to track the deformations. The dashed line creates a distinction between the traditional components of the proposed solution and the experimental components. Sources: [10][14][7]

Chapter 1.2.3 showed that even though a lot of research has already been conducted in the field of MxR, soft tissue biopsy and medical imaging, the technique has not yet been used to visualize and track small MRI-only visible lesions in the female breast. To our knowledge this is the first work that combines the placement of holograms through retroreflective markers, and also implements a deformation model to account for the shape change of the breast when a needle is inserted.

This leads to the main research question this thesis is trying to answer:

How does the success rate of performing biopsy of MRI-only visible lesions in the female breast when using a Mixed Reality guidance system and a deformation model compare with current techniques?

To support the final answer of this question, a set of sub-questions will be answered along with it. These questions are stated below.

1. How accurate can the virtual model of the breast be projected over the real breast?
2. What is the success rate when biopsy is performed using the Mixed Reality lesion model?

1.4 Document overview

The rest of report is structured as follows. Chapter 2 describes the method. It will include information about the internal structures of the individual components and will also describe the experiments that will be conducted. Chapter 3 describes the results of these experiments, chapter 4 will discuss the acquired results, and finally chapter 5 will conclude this thesis and some recommendations for future improvement of the solution will be given.

2 Method

To be able to perform biopsies using MxR, the solution requires three components. The first component is a measurement system. For this, Optitrack will be used and has been described in section 2.1. The second component needs to process the measured data. A Matlab program has been created for this purpose which is described in section 2.2. The final component is a way to visualize the processed data. a combination of the HoloLens & Unity was implemented for this case and its workings are described in section 2.3. Section 2.4 will cover the experiments that will be conducted to answer the research questions.

2.1 Optitrack

2.1.1 Trackable objects

To be able to track an object with the Optitrack system (NaturalPoint, Inc., Corvallis, OR, USA), retro reflective markers have to be attached to the object. These markers are spherical, so that the center of the marker can be identified from every angle. The markers need to be covered in retro reflective material, such that the light that is being shined on the markers will be returned to the light source. The light would be reflected to a random point in space if the marker would be covered with a reflective material instead of a retro reflective one. By including the light source in the camera, the markers will reflect infrared light back to the cameras, enabling the marker to be tracked. This work requires 3 objects to be tracked by the Optitrack System, namely the HoloLens, the ophantom and the calibration square. They will be explained in more detail in sections 2.1.1.1 - 2.1.1.3

2.1.1.1 HoloLens

The first object that was altered to ensure that it can be tracked by the Optitrack system is the HoloLens. A bracket was created in Solidworks (Dassault Systems, Vélizy-Villacoublay, France) such that the spacing between the markers was known. The result is shown in figure 5. The distances relative to the highlighted marker are given in table 2. The orientation of the coordinate frame is also shown in this figure; it is a right handed coordinate frame with its origin at the center of the highlighted marker, and thus the +Y axis pointing outwards of the screen. The bracket was 3D printed on the Ultimaker 2+ (Ultimaker, Utrecht, Netherlands) using Polylactic Acid (PLA).

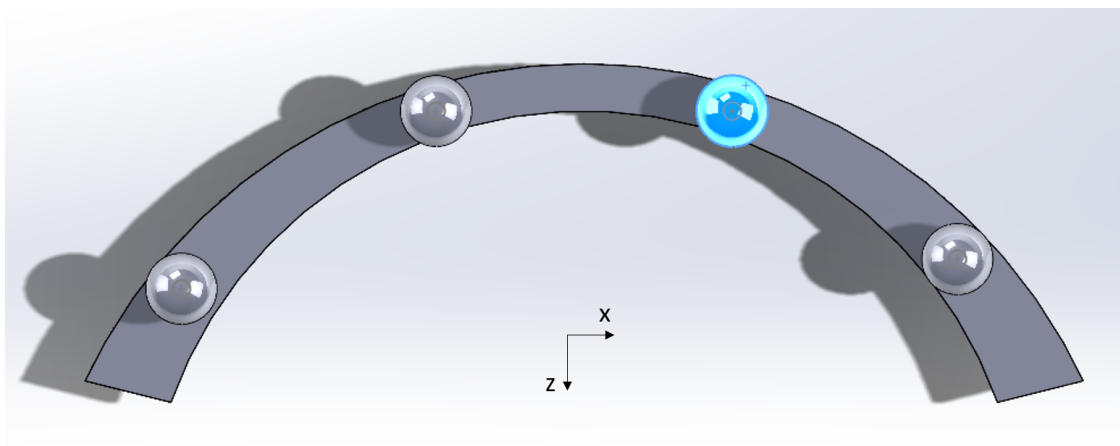


Figure 5: Bracket created in Solidworks. The highlighted marker indicates which marker is chosen as reference point for the HoloLensPivotOptitrack coordinate frame .

The 3D printed bracket mounted to the HoloLens with the retro reflective tape attached to the markers on the bracket is shown in figure 6

Marker Nr.	X (mm)	Y (mm)	Z (mm)
1	38	0	25
2	0	0	0
3	-50	0	0
4	-93	0	30

Table 2: Distances between markers relative to marker 2.



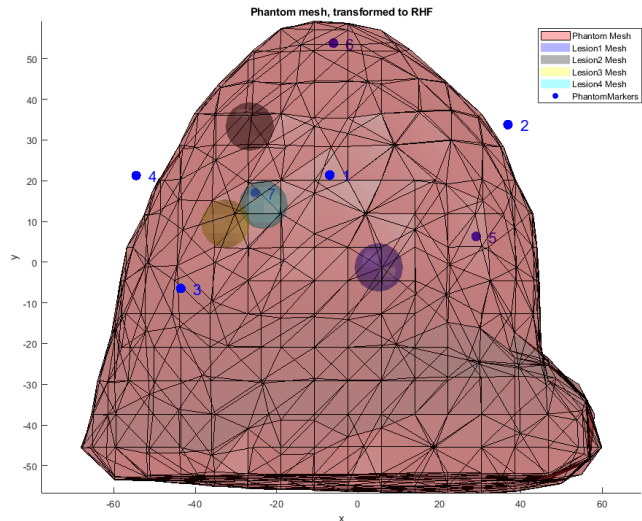
Figure 6: The HoloLens with the 3D printed bracket mounted on top of it. The markers were covered in retro reflective tape by hand such that they can be detected by the Optitrack system.

2.1.1.2 Phantom

The phantom used in this work was created by Tichelaar [39] in his thesis and is created out of PVC plastisol. This substance can be poured in a mold with the desired shape of the phantom. Once the mold cools down the substance will solidify but stays somewhat flexible, which is ideal for the creation of a phantom. The lesions inside the phantom were created from the same material, but by changing the internal ratios the structure of the lesions is stiffer than that of the phantom. The lesions were coloured by adding a dye to make good distinction between the phantom and the lesions. Four lesions were placed at different positions inside the phantom while not being too close to one another. The markers that were attached to the phantom were designed such that they could be detected by both the MRI scanner and the Optitrack system. They contained a mechanism such that they can be removed. Tichelaar [39] investigated the influence of the amount of markers on the phantom and the size of those markers. The outcome of this research was that either six, seven or eight markers can be used with a diameter of 12 up till 20 mm. To minimize overlap but maximize precision, seven markers with a diameter of 12 mm were chosen to be used in this work. Figure 7 shows a side by side comparison of the actual phantom and the phantom created from the MRI data with the seven markers at specific locations to maximize the capture of the deformations of critical parts of the phantom. The positions of the lesions and the markers are given in table 3.



(a) The phantom with relevant markers attached



(b) The mesh of the hologram with the markers and the lesions. The markers that are transparent are located behind the phantom in the current view.

Figure 7: Side by side comparison of the phantom and the mesh created from the MRI data.

Element	X(mm)	Y(mm)	Z(mm)
Lesion 1	5.12	1.27	3.69
Lesion 2	-26.60	-33.33	-9.02
Lesion 3	-32.57	-9.43	6.15
Lesion 4	-23.24	-14.11	33.82
Marker 1	-6.93	39.69	21.41
Marker 2	36.86	8.67	33.79
Marker 3	-43.55	29.63	-6.45
Marker 4	-54.50	-9.37	21.28
Marker 5	29.03	-38.04	6.31
Marker 6	-6.03	-24.55	53.79
Marker 7	-25.25	-47.07	17.07

Table 3: Position data of lesions and markers. All coordinates are described in the right handed coordinate frame which has its origin in the middle of the phantom.

2.1.1.3 L-frame calibration square

The Optitrack calibration square (NaturalPoint, Inc., Corvallis, OR, USA) is an L-shaped frame that was used to define the placement and orientation of the world axis in the camera work space. The orientation of the axis is shown in figure 8, the +Y axis is pointing outwards of the screen.

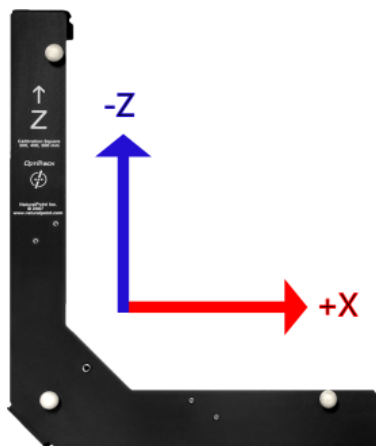


Figure 8: Schematic of the orientation of the axis of the L-frame, +Y is pointing outwards of the screen. Source: [9]

2.1.2 Hardware

The Optitrack setup that was used is available at the Robotics and Mechatronics faculty of the University of Twente. It consists of 11 cameras placed around the ceiling to track objects which have retro reflective markers placed on them. The cameras present in the system are the Optitrack Flex 3 cameras (NaturalPoint, Inc., Corvallis, OR, USA), which are capable of filming at a resolution of 640 x 480 pixels, connecting over USB 2.0 and have a maximum frame rate of 100 Hz. The combination of all the 2D images that these cameras create will result in 3D marker positions in the work space of the setup.

2.1.3 Software

The Optitrack setup uses the Tracking Tools software (NaturalPoint, Inc., Corvallis, OR, USA) from Optitrack. This software is capable of tracking user selected objects that have at least 3 markers in the workspace of the system. The position data can be streamed to external programs or systems. This software package was used to determine the position of the phantom in the work space of the setup. The version of Tracking Tools that was used is 2.5.3. Before the system could be used properly it had to be calibrated. This had to be done since the software needed to determine where each camera is placed relevant to the other cameras. A stick with 3 markers attached to it, the Optiwand 500mm version (NaturalPoint, Inc., Corvallis, OR, USA), was waved through the Field of View (FoV) of each camera and the software determined its position afterwards by means of comparing the data received from each camera per frame.

The software enables the user to change some camera settings like FPS, EXP, THR and LED. FPS defines the frame rate of the cameras and can be selected to be either 25, 50 or 100 frames per second. EXP describes the exposure value which is equal to the time that the camera is exposed per frame. Changing this value will allow either more or less light into the camera. The THR value denotes the threshold value which is used to determine the minimum brightness that a pixel needs to be seen by the camera. A higher threshold value will mean that less bright pixels, which might represent noise, will be filtered out of the output of the camera. The LED setting controls the intensity of infrared light that will be emitted from the LED-ring surrounding the lens of the camera.

The Tracking Tools software enables the user to group markers into a trackable object, that can be tracked by the cameras. The position and rotation of an object with respect to the global reference frame is calculated and send over the network for each individual object. The orientation of an object is of importance when a trackable is created since the rotation part of the homogeneous matrix will be set to have the same orientation as the world frame. The setup that is used in this project to assure correct orientation is shown in figure 9. Using the L-frame calibration square assures that the orientation of the coordinate frames of the trackables equals that of the calibration which is shown in figure 8. The aluminum bars are placed perpendicular to the frame to ease the correct placement of the phantom and the HoloLens relative to the calibration square.

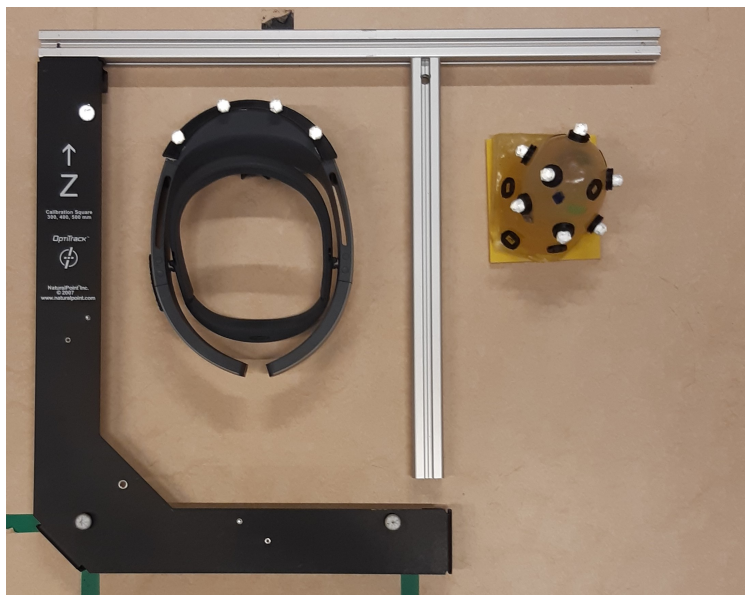


Figure 9: Overview of the physical setup for the alignment of the trackables with the calibration square, HoloLens & phantom.

Each trackable has a lot of parameters that can be altered to improve performance. An important setting that is activated in this implementation is the "Force Exhaustive" setting. This setting forces the software to find the best match for a group of markers instead of finding the first match that has enough resemblance. Enabling this feature makes sure that the markers of the HoloLens will not be assigned to the markers of the phantom, which could happen more often if this feature was not active due to a certain combination of phantom markers sharing geometrical properties with the markers of the HoloLens bracket. Another important setting is the selection of the pivot point of the trackable. Each marker of an object can be selected as the source of the homogeneous matrix. By selecting the marker of the HoloLens according to figure 5, the static transformation between the HoloLens camera and the pivot point can be created to enable a transformation between the HoloLens camera and other coordinate frames in the system.

2.2 Matlab

Matlab (The MathWorks, Inc., Natick, MA, USA) is used as the main processing center of the entire pipeline. A general overview of the structure of the Matlab program is shown in figure 10. The specific function of each of the blocks in the chain will be elaborated on in the subsections below.

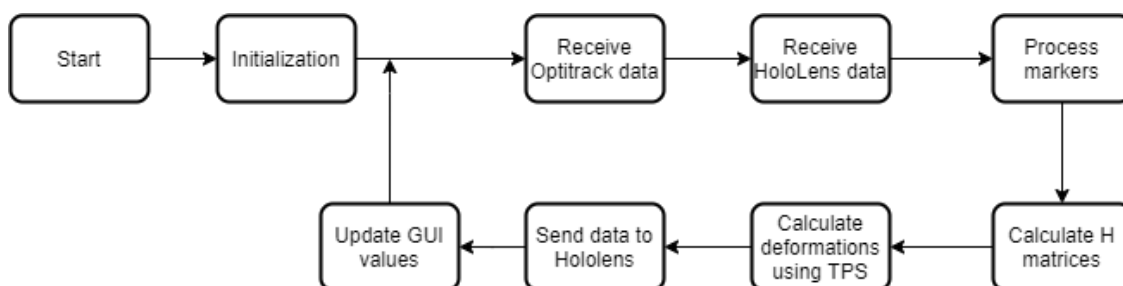


Figure 10: Compact flowchart of the Matlab main program.

Some components of the Matlab program have been implemented in previous research conducted at RaM. Lagomarsino [24] has investigated the usability of the Thin Plate Spline algorithm to map deformations of the breast when looking at the position change of specific reference points, which are the retro reflective markers in this work. The function that she has written to calculate this change will be used in this work. Its functionality is described in section 2.2.5. Tichelaar [39] has implemented the functions that house the matching algorithms. These functions will process the marker data. Their functionality has been described in section 2.2.4. Some changes have been made to the functionality of those functions to account for the

scenario in which more markers are detected than expected. These changes are also described in section 2.2.4.

2.2.1 Communication with Optitrack

The communication with the Optitrack software, Tracking Tools, is established using NatNetSDK (NaturalPoint, Inc., Corvallis, OR, USA), which is a software development kit to acquire data over a network connection. The client has to connect to the computer which is recording the data by entering the IP addresses of the client and the server. Whenever a connection is made, the server transfers the marker positions and relevant data for selected objects in Optitrack (Name, H matrix, Timestamp). Due to the outdated software version, extra functionality like an option that already assigns the markers to a specific object in Optitrack could not be used. The NatNetSDK uses the UDP protocol to send out data with as little delay as possible. The communication with the Matlab program is one way communication since the Matlab program only receives data and does not send any data to the Optitrack System.

2.2.2 Communication with HoloLens

To communicate with the C# program running on the HoloLens, a way to ensure correct data transfer was implemented. The two programs connect via a TCP connection on a single port, that way a single TCP/IP thread can run on the HoloLens to account for all communication. TCP was used since receiving all of the data correctly has a higher priority than speed in the current implementation of the solution. A system was used that employs headers to indicate which type of data is being send. Each transmission consists of three parts, which are explained below.

1. Header

The header is the main identification element which tells the C# program what type of data it can expect. This data will be received and entered into a switch statement to open the correct function for processing the rest of the data that will be sent.

2. Buffer Size

The buffer size is send over the network to enable the C# program to construct a data object that is large enough to store all of the data that will be send. Different headers will result in different data types and array sizes that all have to be accounted for by the HoloLens program. The data that is send will either be single precision (32 bits) or int32 (32 bits).

3. Data

The actual data is the final step of the communication process. The Matlab data is stored in arrays and the program will send the entire array in a single instance. Data which includes decimal numbers is send in single format and data which only consists of integers is send as int32 format. Both types need four bytes (32 bits). Whenever an array consists of more than 1400 bytes (350 items), Unity will read the data from the socket in chunks of 1400 bytes due to the Maximum Transmission Unit (MTU) of Ethernet. The C# program will loop over the buffer and remove 1400 bytes until the buffer is empty. Afterwards it will rewrite the received data to either single or int32 type and store it in the correct variable for further use in the program.

2.2.3 Homogeneous matrix

Since the trackable objects are defined in different coordinate frames, a system was implemented to link these objects. There are various methods to do this, but this work uses homogeneous matrices.

$$H_0^1 = \begin{bmatrix} R^{3 \times 3} & t^{3 \times 1} \\ 0^{1 \times 3} & 1^{1 \times 1} \end{bmatrix} \quad (1)$$

A homogeneous matrix consists of a rotation and a translation to describe the position of a point, defined in frame 0, in frame 1. The layout of this type of matrix is given in equation 1. The notation H_0^1 is used to describe a transformation from frame 0 (lower index) to frame 1 (upper index). The matrix consists of a rotation part, R, which is a 3x3 matrix and a translation part, t, which is a 3x1 matrix. To be able to multiply these matrices, a row of [0 0 0 1] is added to the bottom of this matrix to make it a square 4x4 matrix. This is a very useful property since the matrices can be chained to describe a transformation between two coordinate frames using known transformations between intermediate frames, as is shown in equation 2.

$$H_0^n = H_{n-1}^n \dots H_1^2 H_0^1 \quad (2)$$

The general overview of the coordinate frames and their orientation is shown in figure 11. For an extensive overview of all relevant coordinate frames that were created, transformation matrices between those frames, and the multiplications that were applied, the reader is referred to Appendix A: Homogeneous matrices.

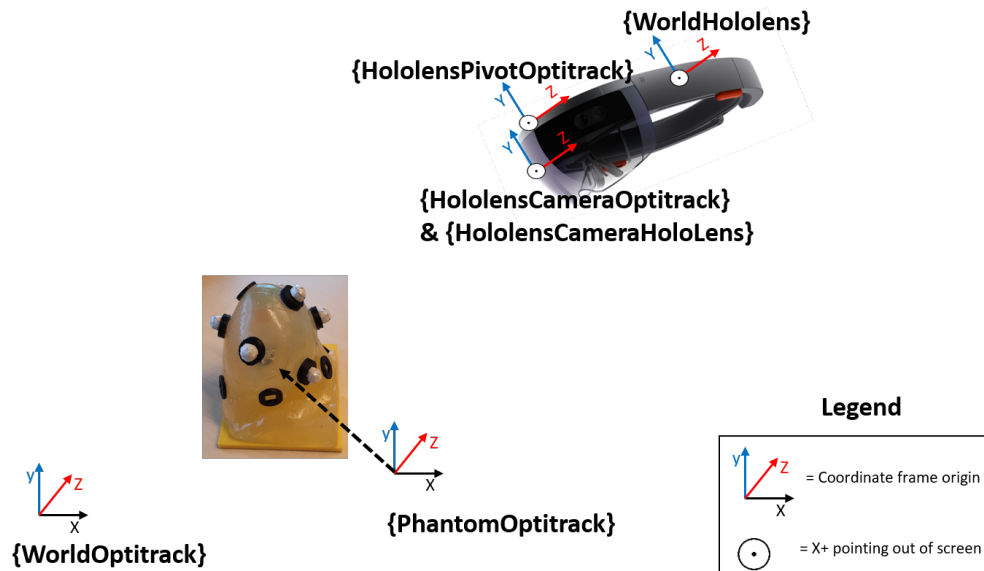


Figure 11: Overview of the different coordinate frames and their orientations. Each frame with a HoloLens subscript should have the orientation of the z-axis flipped since it is a left handed coordinate frame. This is not shown in the figure since it would make the image messy and unclear.

2.2.4 Marker identification

The only information that the Matlab program receives from the Optitrack system about the markers is their position with respect to the origin of the camera system. These positions are received as a $n \times 3$ matrix where n is the amount of markers that have been detected by the cameras. This information has to be processed to assign a specific marker to their corresponding object, since the markers in the matrix are not sorted in any way. The implementation that has been adapted to overcome this problem, designed by Jiménez Bascones et al. [21], was implemented by Tichelaar [39] in his research and has been altered to function correctly in this work. The markers were tested on three properties, namely the distance between two markers, the angles of a triangle which will be formed from three markers and the height difference between two markers. A fourth algorithm was developed in the work of Jiménez Bascones et al. [21] which compares the similarity ratio between four markers. Tichelaar [39] showed that it did not improve the outcome compared to the other three properties, so it was not included in this work.

Before all markers will be matched using the matching algorithms, a filtering step will take place to filter out irrelevant markers that can be classified as noise. This will be done by creating a region around the origins of the coordinate frames PhantomOptitrack and HoloLensPivotOptitrack, which are both received from the Optitrack system based on the positioning and orientation of the trackable objects. This functionality will filter out marker data that is not close to one of those objects and thus is not a marker of such object. It will also divide the general marker matrix in two object specific marker matrices. The second function will assure that markers from the phantom will not be matched to markers of the HoloLens and vice versa. The filtered marker matrices can however still include faulty marker amounts, since noise might be picked up close to the object. Therefore, the need to further process them by using the matching algorithms keeps existing. The filter region for the phantom has a spherical shape since the coordinate frame is located within the center of the phantom. The filter region for the HoloLens has an ellipsoidal shape, since the markers of interest are always located at the same y position when the markers are described in the HoloLensPivotOptitrack frame. An ellipsoid is chosen to take advantage of the geometric properties of the marker bracket of the HoloLens, and thus filter out more faulty markers early in the program.

Since the amount of markers that can be received for each object can have three states, it is either lower, equal or higher than the expected amount of markers, the identification functions will have to account for these three states. The algorithm in 2.2.4 states the working of the algorithm when the correct amount of markers have been found. The only difference with the other two states is that these will have an extra step up front that will find which marker is occluded/added by comparing the interquartile range of the markers of the current iteration to see which marker is added/removed compared to the last iteration. Each of the three algorithms uses the same layout. The only difference is the algorithm that is assigned in the first step of the program, which is the relevant outcome for a specific matching task.

Algorithm 1 Pseudocode of Marker Identification

Available data: D_L XYZ object marker data of last iteration, D_C XYZ object marker data of current iteration.

Start

Create relevant matching object using D_L

Create relevant matching object using D_C

for n markers **do**

Reshape error result matrices to match remaining number of markers n ;

for k distances **do**

calculate spreading with other markers using interquartile range;

end for

Select marker with biggest spread: \mathbf{b} ;

for n markers **do**

Calculate RMS error of \mathbf{b} with all D_L ;

end for

Map marker with lowest error to \mathbf{b} ;

Update matrices to occlude any row or column that has \mathbf{b} as an option;

Save \mathbf{b} to the output matrix;

$n = n - 1$;

end for

Return: Output matrix of options which marker of current iteration matches the same marker in the last iteration.

Each algorithm will produce an output list which will result in a $n \times m$ matrix, where n = the number of markers and m = the amount of used algorithms. This matrix stores the output of each of the identification algorithms to what marker of the last iteration the marker in the current iteration is linked. An example of such matrix is shown in equation 3. Marker 1 of this iteration is linked to marker 5 of last iteration, marker 2 is linked to marker 7 of last iteration etc.

$$\text{output} = \begin{bmatrix} 5 & 5 & 5 \\ 7 & 7 & 7 \\ 8 & 3 & 8 \\ 1 & 1 & 1 \\ 6 & 6 & 6 \\ 3 & 11 & 3 \\ 10 & 10 & 10 \\ 4 & 4 & 4 \\ 11 & 8 & 11 \\ 2 & 2 & 2 \\ 9 & 9 & 9 \end{bmatrix} \quad (3)$$

Equation 3 shows that the outputs of the algorithms is not always the same. Whenever this occurs the output that is chosen by two out of three algorithms is chosen to be the correct one. Whenever each algorithm assigns a different marker, each marker that is assigned by two of the algorithms is removed from the list and the list is updated to remove these options. If afterwards an unique output can still not be created, the entire measurement will be discarded and the current loop program of the Matlab program will be terminated, forcing it to start over again with a new measurement.

2.2.5 Thin Plate Spline (TPS)

TPS is a smooth interpolation method that considers the bending of a thin sheet of metal. The bending is done according to a given group of set points and the algorithm aims to minimize the energy needed to perform the bending [34]. Using this method will allow the mesh of the phantom and the position of the lesions to be mapped to a new location whenever the phantom is deforming. This implementation of TPS uses the 3D locations of the phantom markers in both the phantom frame and the Optitrack frame to transform a set of points from the phantom space to the Optitrack space and also account for any deformations.

The process is done in two steps. In the first step the parameters \mathbf{w} & \mathbf{a} will be calculated. \mathbf{w} describes the weight factors of the solution and will map the non-linearities in the solution and \mathbf{a} describes the linear affine transformation coefficients. The matrix \mathbf{L} is created to map the input data to \mathbf{w} & \mathbf{a} and is shown in equation 4. Matrix \mathbf{K} holds the pairwise distance between the phantom markers of the MRI scan and is symmetric. \mathbf{P} stores the 3D coordinates of the phantom markers of the MRI scan with a column of one's added as first column.

$$\mathbf{L} = \begin{bmatrix} \mathbf{K} & \mathbf{P} \\ \mathbf{P}^T & \mathbf{0}^{4 \times 4} \end{bmatrix} \quad (4)$$

\mathbf{L} can be used to calculate \mathbf{w} by multiplying its inverse with \mathbf{V} , which houses the 3D marker location data of the frame that the lesion should be mapped to. \mathbf{a} can be calculated by multiplying the inverse of \mathbf{L} with a block of zero's, as is shown in equation 5.

$$\begin{bmatrix} \mathbf{w} \\ \mathbf{a} \end{bmatrix} = \mathbf{L}^{-1} \begin{bmatrix} \mathbf{V} \\ \mathbf{0}^{4 \times 3} \end{bmatrix} \quad (5)$$

When \mathbf{w} & \mathbf{a} are known the second step of the algorithm will be executed. Equation 4 will partly be used again to recalculate \mathbf{L}_2 . The main difference being that the output only is a single matrix this time, so only the upper part of \mathbf{L}_2 will be used. \mathbf{K}_2 will contain the inter-marker distance between the phantom markers of the MRI-scan and the markers retrieved from the Optitrack system. \mathbf{P}_2 now houses the 3D coordinates of the data that is to be transformed, again with a column of ones added as the first column. This can be either the vertices of the mesh or the lesion coordinates which both are $n \times 3$ matrices. The updated matrix \mathbf{L}_2 can be multiplied with parameter vectors \mathbf{w} & \mathbf{a} to output a final matrix \mathbf{Y} which will include the updated positions of the mesh or lesions as shown in equation 6.

$$\mathbf{Y} = \mathbf{L}_2 \begin{bmatrix} \mathbf{w} \\ \mathbf{a} \end{bmatrix} \text{ with } \mathbf{L}_2 = [\mathbf{K}_2 \quad \mathbf{P}_2] \quad (6)$$

2.2.6 Graphical User Interface (GUI)

The GUI has been developed to visualize certain outputs of the program in real time. An overview of the GUI is shown in figure 12.

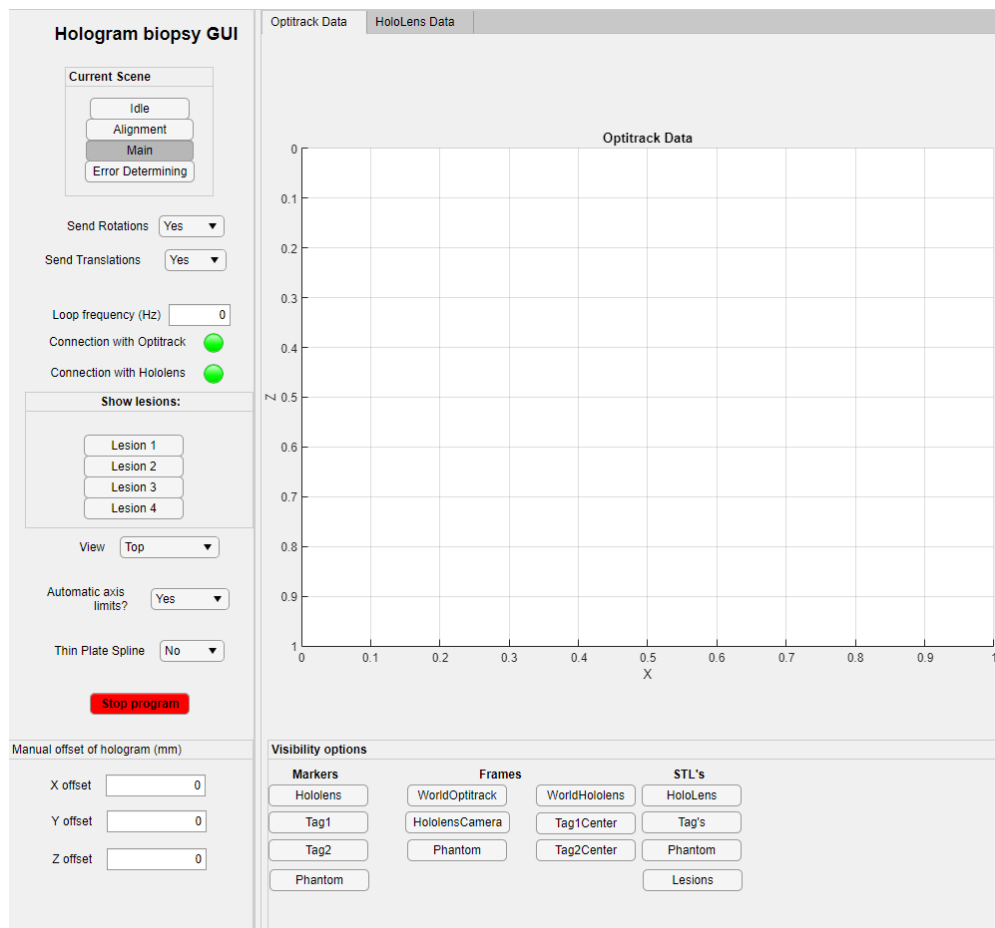


Figure 12: GUI to control and visualize the Matlab program

The left side of the GUI houses the buttons that can be used to swap between different scenes in Unity, the Matlab program will swap accordingly. This way the operator can control both the HoloLens and the Matlab program from the PC. These scenes have mainly been used for testing and the final solution only uses the main scene, which is the default scene loaded when the program is started.

The status lights indicate whether the communication between all components is still available. The loop frequency tracks the time it takes the program to complete all the calculations in a single loop of the program. The lesions tab allows the operator to select which lesion is to be projected in the hologram. The view tab allows for the data in the axis to be viewed from a different angle. The Thin Plate Spline (TPS) allows for the activation of the deformation algorithm. Finally, a stop button was implemented that will shut the program down. The value boxes at the bottom of the panel can be used to manually align the hologram if the position has to be changed by the operator.

The right panel houses a pair of axis which is used to plot all graphical components. The buttons on the bottom are used to enable or disable visualization of specific markers, coordinate frames and STL's. These will all be plotted in the WorldOptitrack coordinate system which matches the real life situation in the camera lab.

2.3 Unity

Unity (Unity Software Inc., San Francisco, CA, USA) is a game engine that uses the programming language C# (C-sharp), which is a programming language developed by Microsoft. It has been designed to be a simple, object-orientated and modern programming language [12]. Unity was used to create a hologram from the model data received by the Matlab program and to project the hologram at the desired position. The version of Unity that was used in this project is 2019.4.17f1. To be able to create MxR applications in Unity, the Windows Mixed Reality Toolkit (MRTK) had to be imported into the project. This is a toolkit developed by Microsoft to ease the creation of apps on the HoloLens by adding MxR specific features and setting to an Unity project.

Holograms in Unity are created from meshes. A mesh is a collection of triangles and can have any shape or size. Such mesh consists of a list of vertices, which describe points in 3D space, and a list of triangles which describes between which three points in the vertices list a triangle has to be drawn. By combining this information the shape can be drawn in Unity and thus an object can be represented in 3D. Whenever the shape of a mesh changes, all that needs to be done is to update these two lists and the new shape will be drawn. The mesh of the phantom will consist of a mesh for the breast and four meshes for the lesions. This way each individual lesion can be turned on or off and gives the operator the control which lesion is going to be selected for the biopsy. All lesion meshes are made children of the game object which describes the position and orientation of the phantom mesh. This is done such that whenever the phantom is rotated or translated all of the lesions will follow this movement and their position relative to the phantom will not have to be updated individually.

The program consists of a main thread that is used to display the meshes of the phantom and lesions and a TCP/IP thread that is used to communicate with the Matlab program. The Matlab program will send headers to identify which data is being sent and the Unity program will place the received data in the correct variables, as is described in section 2.2.2. The data that is sent from Matlab to the C# program are vertices and triangles for both the phantom and the lesions, rotation and translation of the phantom, scene switch commands, and the termination signal. The HoloLens will send its position relative to the world frame of the HoloLens back to Matlab, which will be used to place the hologram. The main thread will check whether any of the parameters have been updated and will process the data accordingly. A flowchart of the main & TCP/IP thread is shown in figure 13.

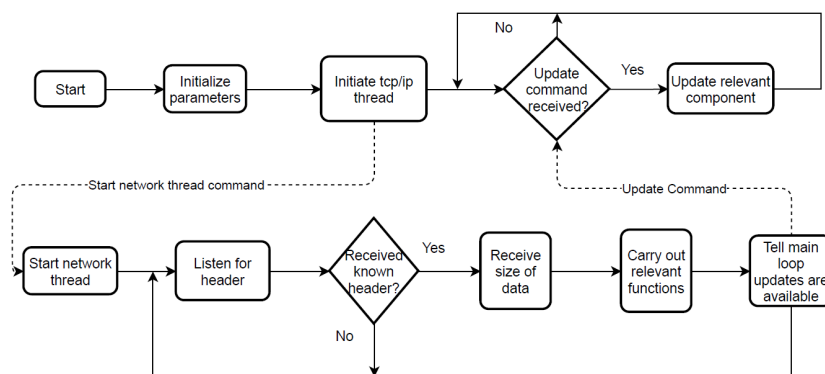
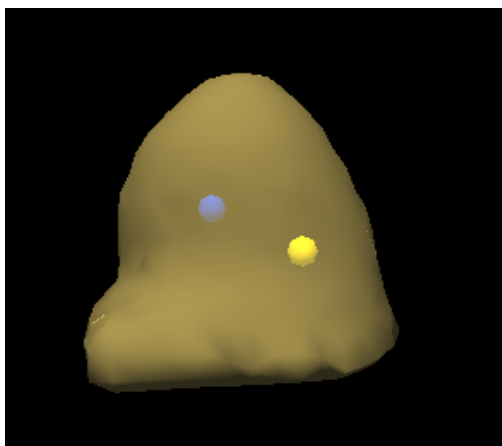


Figure 13: Compact flowchart of the Unity main program (top) and the network thread (bottom).

The generated hologram and the floating menu is shown in figure 14. The floating menu consists of a slider to change the transparency of the phantom hologram and buttons which have mainly been used in the development of the program and are not of importance for the final solution.



(a)



(b)

Figure 14: Screenshots of the rendered hologram with lesion 1 and 2 enabled (a) and the floating menu(b).

2.4 Experiments

This section explains the experiments that were conducted to answer the research questions of this work. The general workflow of each experiment is described below, specific settings for each experiment are described in sections 2.4.1 - 2.4.4.

A stand for the HoloLens was created and 3D printed by altering the design of B. Bauerly [8]. This stand created a static transformation between the PhantomOptitrack and the WorldHoloLens frame. The stand places the HoloLens at a known position from the center of the phantom and because the HoloLens is in this position when the program is started, the WorldHoloLens frame will be placed at a known position relative to the HoloLensCameraOptitrack frame. The hologram is placed in the WorldHoloLens frame once at the start of the program and the HoloLens keeps the hologram at the right position while the person wearing the HoloLens is moving around with it. The stand with the HoloLens and the phantom attached to it is shown in figure 15.



Figure 15: HoloLens stand connected to the phantom. The stand can be attached to any of the 4 corners of the orange plate on which the phantom is placed.

The first component that has to be launched is the Optitrack system. The operator has to select the correct file which includes the camera calibration and the trackables with the correct orientation. Afterwards the Matlab program will be started and will create a connection with Optitrack. At last the Unity program will be started using the Windows Device Portal (WDP) (Microsoft, Redmond, WA, USA) which is a web server that allows the operator to control certain parts of the HoloLens, like taking a picture or video, starting apps, and download data of the HoloLens via WiFi or USB. The operator will start the application while the HoloLens is still in the stand. Once the first iteration of the Matlab program is completed and the hologram is placed, the user can pick up the HMD and place it on his/her head for usage.

2.4.1 Hologram placement error evaluation

The first experiment that was conducted evaluated the error of the hologram placement. It also validated the correct implementation of the chaining of homogeneous matrices

To evaluate the error that was still present when placing the hologram on top of the phantom, a ruler was placed next to the phantom. The user looked at the hologram from the x,y & z direction and pictures were taken using the HoloLens camera. Because the scale of the ruler was in the same picture as the hologram, the pixel-wise difference could be calculated and transformed to millimeters.

Another aspect of the hologram placement that was evaluated is the rotational error. The phantom and HoloLens were placed in different starting positions to verify whether a different starting position results in a different orientation of the hologram.

2.4.2 Marker filtering

The second experiment investigated the influence of the marker filtering step. The filtering step was evaluated by running the program with and without this feature enabled to look at the outcome of the marker matching algorithms and to confirm that the supplied list of matched markers corresponds to the real life situation.

2.4.3 Thin Plate Spline validation

The third experiment evaluated the TPS algorithm. The outcome of the TPS was visualized in a simulation to show the working of the principle in Unity. The phantom was moved by pressing against it in a known direction. The experiment was conducted with the HoloLens both being turned on and off to look at the influence of the infrared light emitted by the HoloLens.

Finally the HoloLens was worn by a user and the deforming hologram could be reviewed in real life. The screens of the operator were recorded to be able to look back at the data to see whether unexpected behaviour occurs. When the HoloLens was being worn, a video was taken of the situation to visualize the output of the HoloLens.

2.4.4 Biopsy

The final experiment that was conducted was performing a biopsy using the created implementation.

Biopsy was performed on each lesion 12 times, three times per direction facing either positive or negative x or z when looking at the orientation of the WorldOptitrack coordinate frame. This was done to evaluate the correct placement of the hologram in 3D space. A schematic showing the positions of the lesions, phantom, HoloLens & the directions from which the biopsy was performed is given in figure 16.

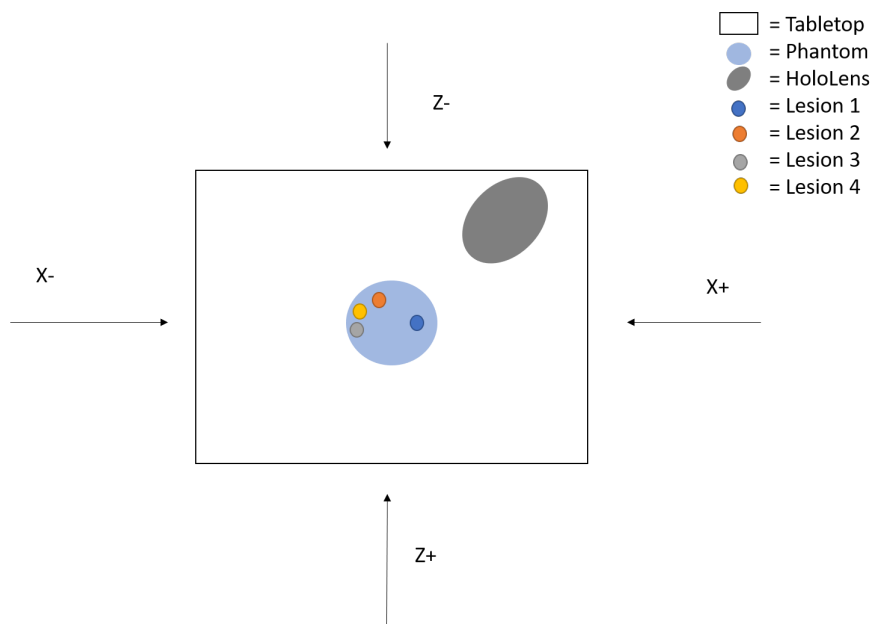


Figure 16: Schematic overview of the biopsy experiment setup. The direction specifies the position in the WorldOptitrack frame from which the biopsy will be performed. The user will always orientate his/her head to the opposite side to look at the phantom & the hologram.

The entire procedure was performed twice, once with and once without the TPS enabled to evaluate the influence of the deformation modeling. The biopsy could have three outputs; either it was successful when the lesion was hit, failed when the lesion was not hit, or was considered a technical fail when the biopsy could not be performed due to limitations caused by the implemented solution. The last option can only happen when the TPS algorithm was used, since wrong marker identification could distort the hologram such that it was unusable and a biopsy could not be performed.

The starting position of the HoloLens and the phantom will be the same in all biopsies to be able to evaluate the results regarding the placement of the hologram in 3D space.

The transparency of the hologram was set to 0.5 on a scale from 0 to 1. This value was chosen such that the insides of the phantom were not visible when the hologram was projected over the phantom, but the user was still able to see the position of the needle relative to the projected lesion. Using a higher transparency would not allow the user to see the needle since the HoloLens would block it by projecting the hologram with a high intensity of light. Using a lower transparency would allow the user to actually see the insides of the phantom and to look at the lesion that had to be targeted in real life instead of only through the hologram.

The second setting that was changed to carry out this experiment was the cull mode. Back-face culling will determine whether a triangle of a mesh is visible in the line of sight of the camera and otherwise will not render the triangle to improve performance of the program. Changing this setting in the phantom mesh to front-faced culling enabled the meshes of the lesion to be drawn over the mesh of the phantom instead of behind the phantom mesh. This enabled the program to visualize both the hologram to fade out the inside of the phantom and to let the mesh of the lesion of interest stand out such that it could be tracked by the user.

The biopsies were performed using the biopsy gun shown in figure 17. The device shown is a semi automatic biopsy gun (Invivio Corporation, Gainesville, FL, USA) with a 14G (1.6mm) needle which has a length of 100 mm to extract tissue by sliding the outward cannula over the hollow portion of the needle, encapturing the tissue in the needle and ensuring the tissue can be extracted.



Figure 17: The biopsy gun used in the experiments.

3 Results

This chapter describes the results acquired from the experiments described in section 2.4. Section 3.1 describes the results of the hologram placement, section 3.2 shows the results of the marker filtering, section 3.3 contains the results of the TPS algorithm and finally section 3.4 describes the results obtained from the biopsies.

3.1 Hologram placement

The first experiment that was conducted was done to evaluate the error of the phantom placement. Figure 18 shows the errors in all 3 dimensions, the values have been acquired by measuring the difference between equivalent hologram and phantom faces and have been noted down in table 4. A visualization of the distribution of the error is given in the box plot shown in figure 19.

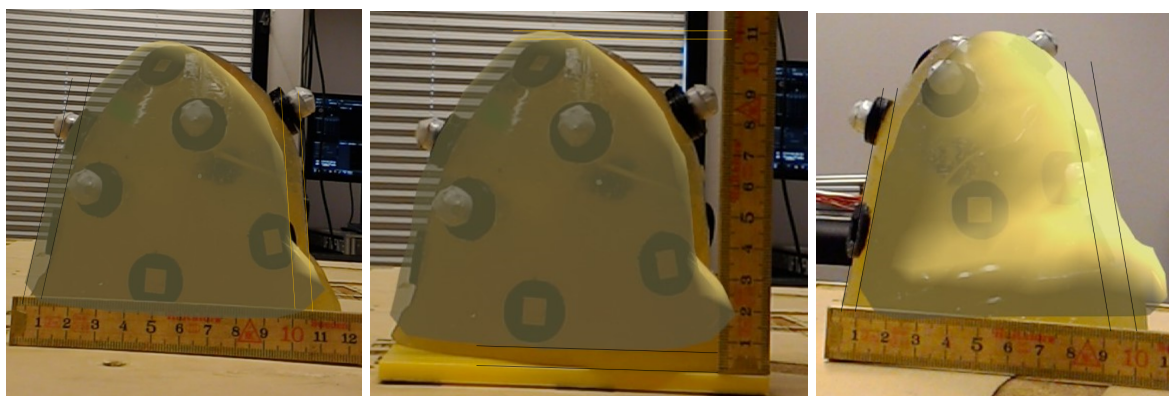


Figure 18: Hologram error evaluation of the X (left), Y (middle) and Z (right) axis in mm.

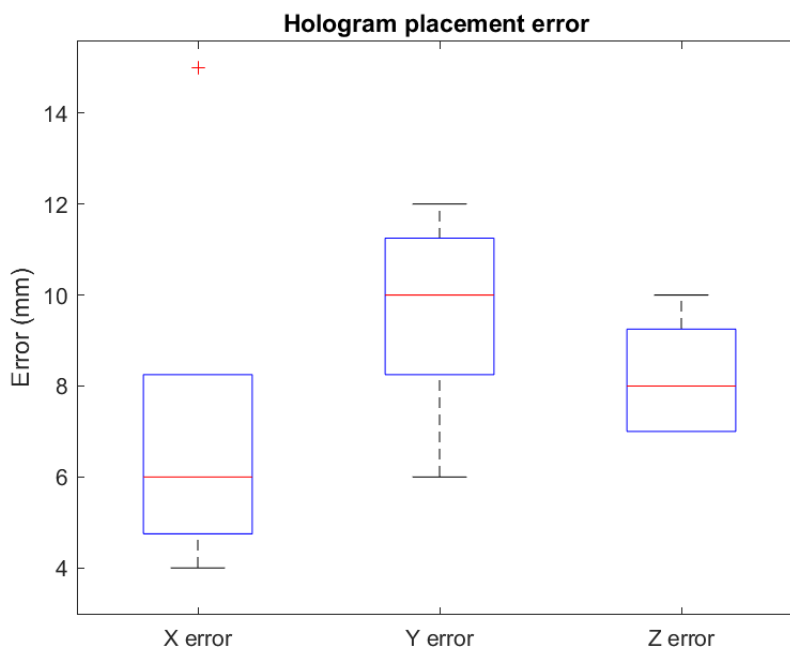


Figure 19: Boxplot of hologram placement error measurements in X,Y&Z direction.

Error	X	Y	Z
With outliers	7.2 ± 4.4	9.6 ± 2.3	8.1 ± 1.3
Without outliers	5.3 ± 1.0	9.6 ± 2.3	8.1 ± 1.3

Table 4: X,Y & Z error of the hologram placement compared to the phantom. Values are given as mean \pm standard deviation over 5 measurements and in millimeters

Figure 19 shows that an outlier is present in the x-error data. Removing this error will result in $E_x = 5.3 \pm 1.0$ instead of 7.2 ± 4.4 .

The influence of the starting position of the phantom and the HoloLens has also been researched. Figure 20 shows two different starting positions and next to them two outcome's of the hologram placement.

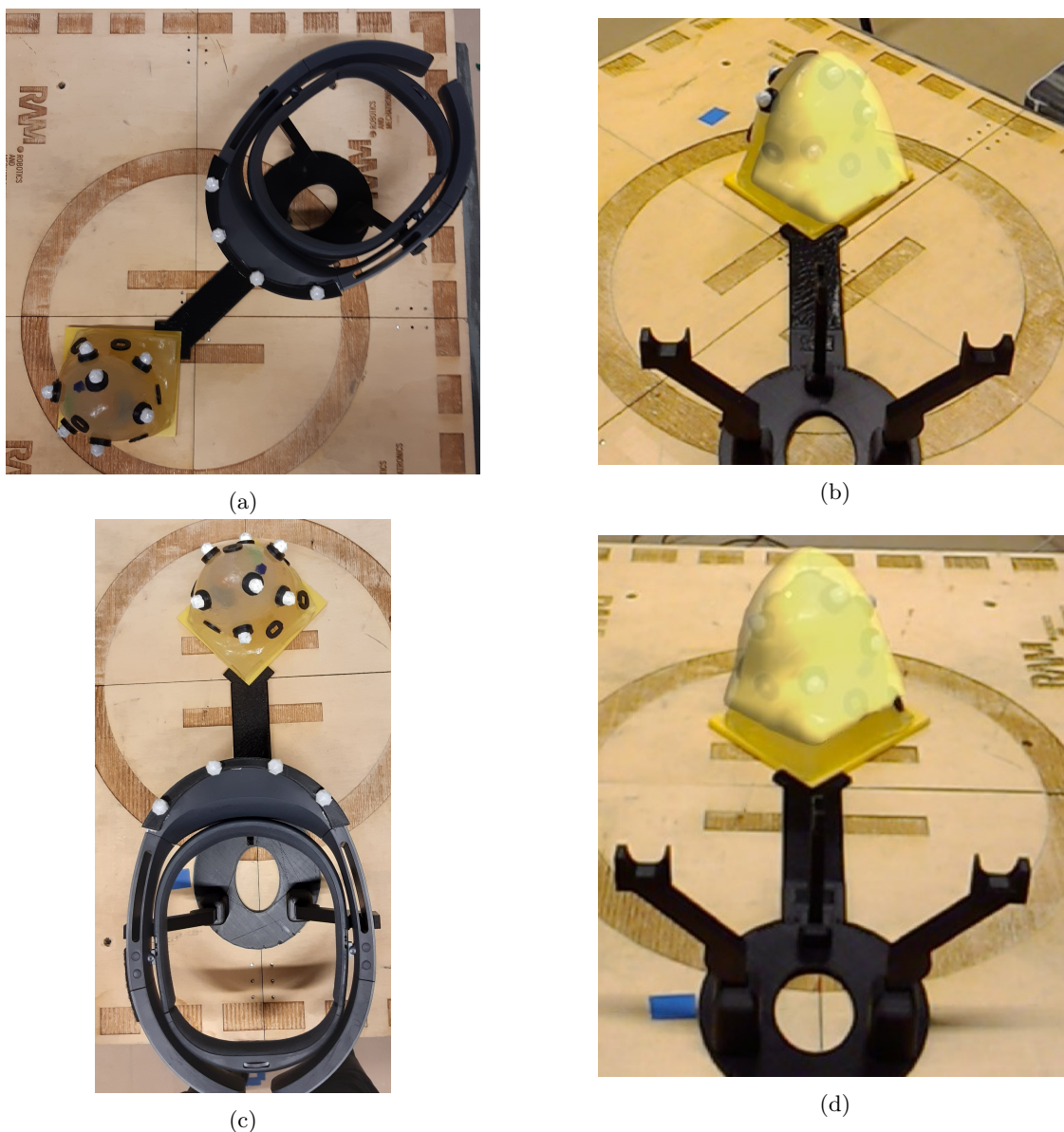


Figure 20: The first setup photographed from above (a), the resulting hologram (b), The second setup photographed from above (c), the resulting hologram(d). The difference in starting orientation can be deduced from the changed orientation of the helicopter sign on the tabletop.

The error present in figure 18 can be accounted for. Figure 21 shows the hologram being placed on top of the phantom while being positioned with a manually entered offset vector. The entries in the offset vector

are the same as the values given in table 4.

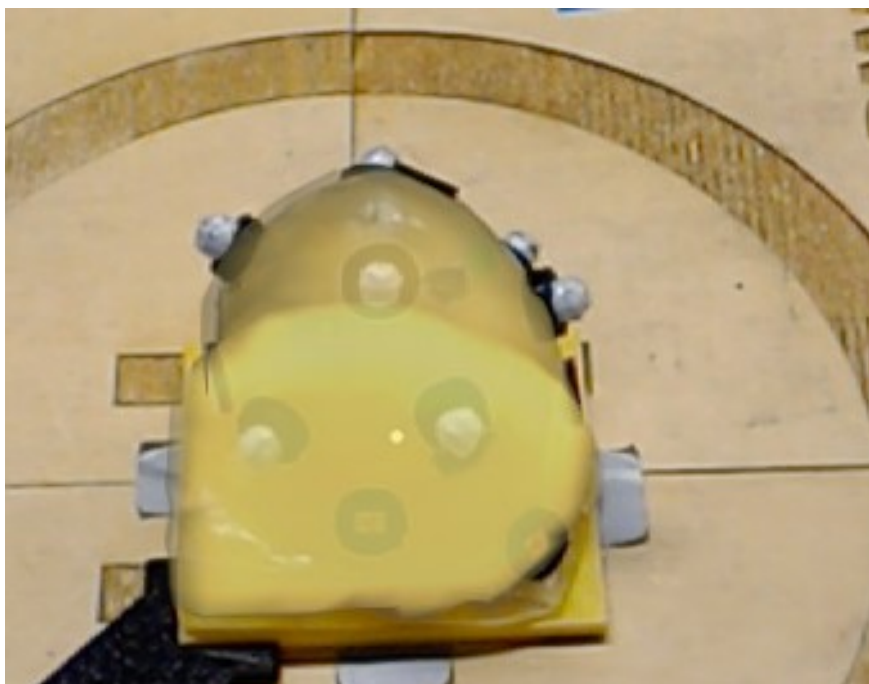


Figure 21: The hologram being projected on top of the phantom with the offset vector

3.2 Marker filtering

Before all markers were processed, a filtering step was added to only allow markers within a certain radius of the origin of the coordinate frames of either the phantom or the HoloLens. A graph showing the outcome of this filtering is shown in figure 22. The radius of the spherical filtering region for the phantom is 90 mm and the radiuses for the ellipsoidal filtering region (FR_x, FR_y, FR_z) = (130, 80, 20), all in mm. These radiuses were used to determine the region surrounding the coordinate frame origins, PhantomOptitrack for the phantom and HoloLensPivotOptitrack for the HoloLens, that would still include relevant markers as is also described in section 2.2.4. The markers that were occluded from further calculations are colored black, the phantom markers are colored red and the HoloLens markers are colored blue.

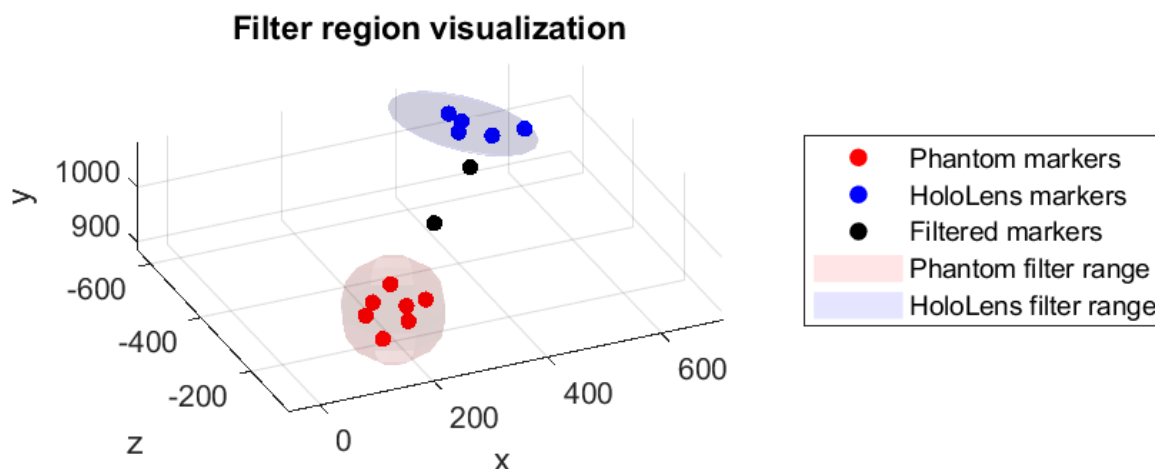


Figure 22: Visualization of the filter regions of both objects.

The impact of the filtering step is shown in figure 23. The same marker data was used for the creation of both graphs. The figure shows that, without the filter, markers of the phantom can wrongfully be assigned

to the HoloLens. This does not occur when filtering is enabled due to the limited options the matching algorithms have.

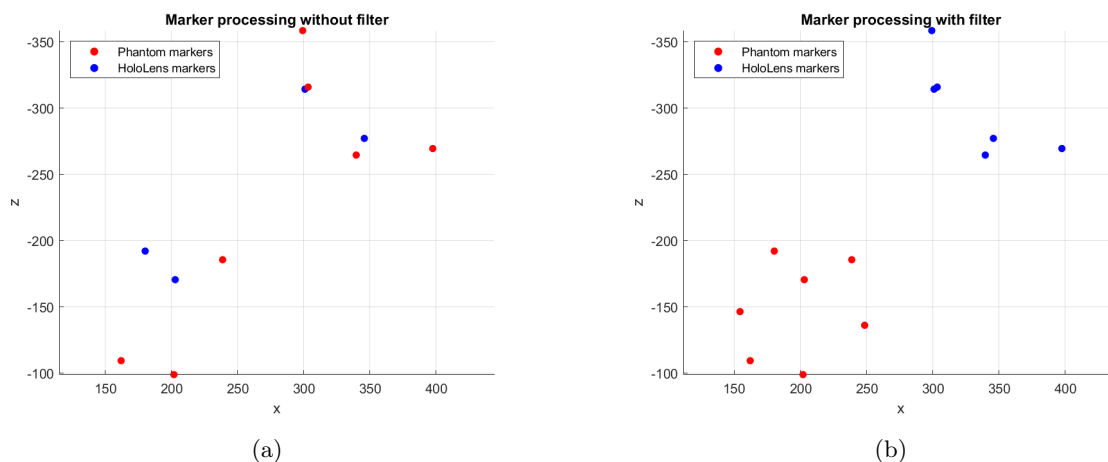


Figure 23: Marker matching results with the filtering turned off (a) and turned on (b)

3.3 Thin Plate Spline (TPS) validation

The validation of the correct functioning of the TPS method is done in three parts. The first part was done by means of a simulation to show the correct working when the HoloLens was turned off. The results are shown in figure 24 & 25.

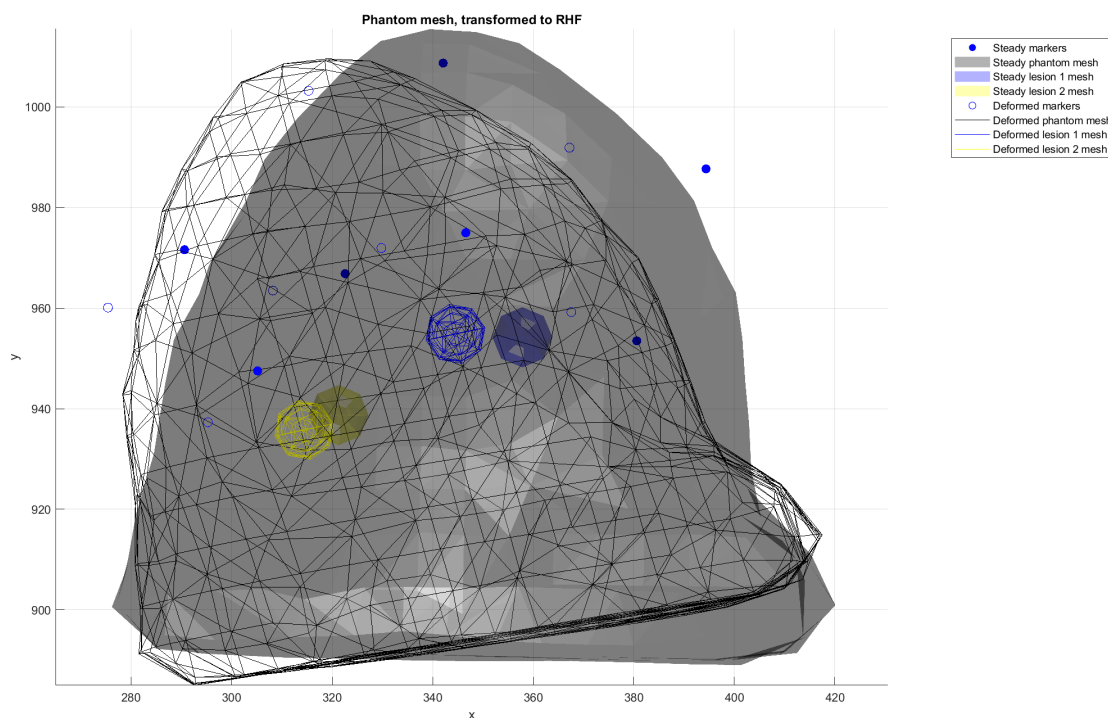


Figure 24: Visualization of TPS when a force is applied from $x+$ to $x-$ direction. The filled meshes are the original positions and the outlined meshes and circles represent the same components after their position is recalculated.

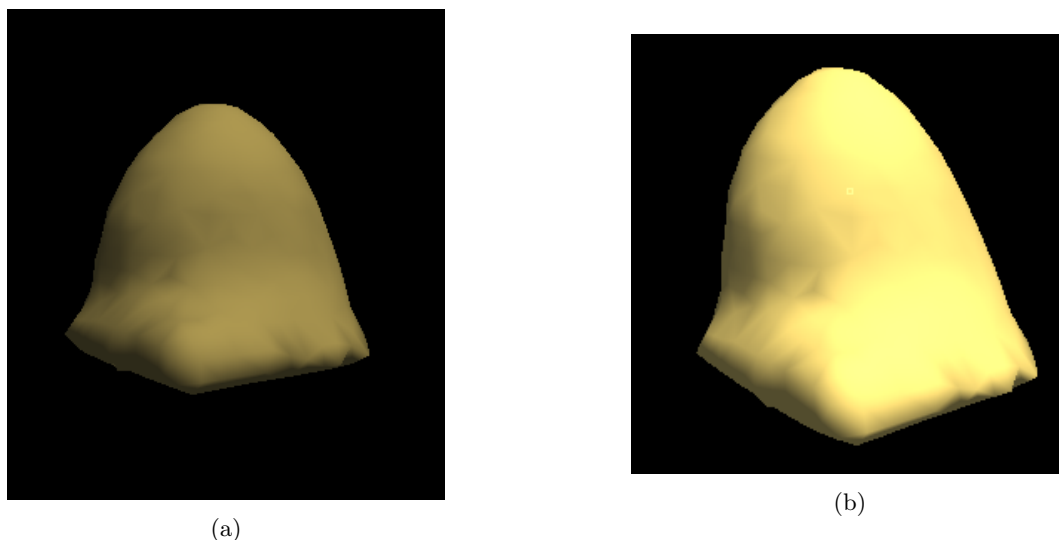


Figure 25: The Unity simulation showing the phantom at rest (a) and when it is being pushed in positive x direction (b)

Whenever the HoloLens was turned on, extra infrared noise was added to the system and the influence on the solution was investigated.

The system would sometimes match the correct markers to the correct objects but would mismatch markers within an object, this is shown in figure 26. The markers from the current iteration of the program are in a different order than those off the original scan and this results in the algorithm warping around the mesh.

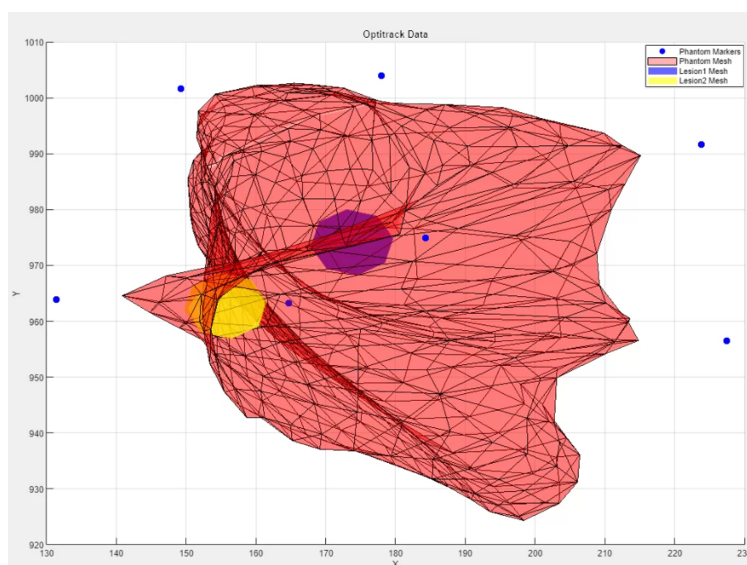


Figure 26: Visualization of incorrect TPS calculation

The effects of the TPS algorithm have also been reviewed when used on the actual phantom. Figure 27 shows a side by side comparison of two screenshots from a video taken while the operator was pushing the phantom. Especially the top of the hologram moved to the side when the phantom was pushed, but this might be hard to see due to the misalignment of the hologram with the phantom. It can be seen more clearly when looking at the position change of the lesion, which changed considerably when comparing the left figure to the right.

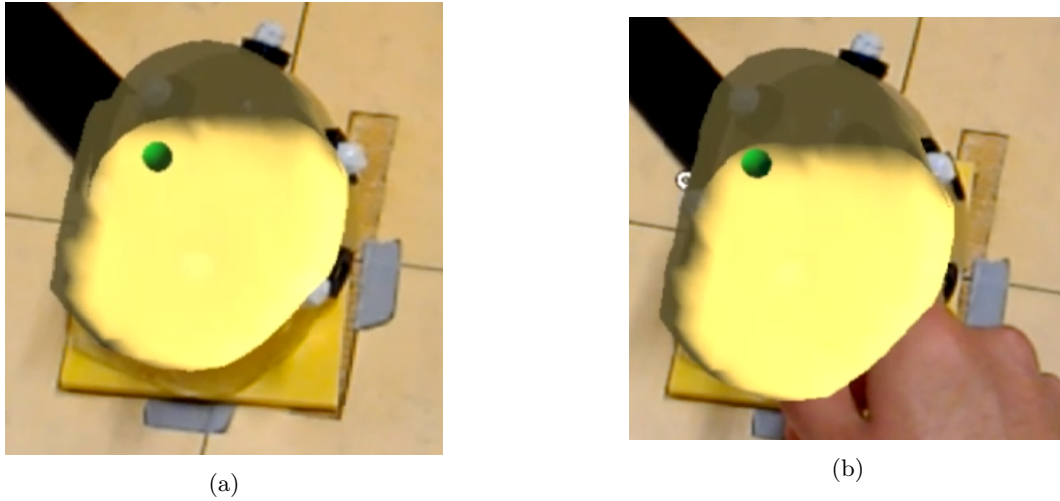


Figure 27: Screenshots from a video showing the working of the TPS algorithm while stable (a) and while the phantom is being pushed(b).

3.4 Biopsy

The results of the 72 performed biopsies are shown in this section. Figure 28 shows the results from the biopsies when the TPS algorithm was turned off and figure 29 shows the results when the algorithm was turned on. The graphs show the results of the biopsies grouped per direction from which the biopsy was performed.

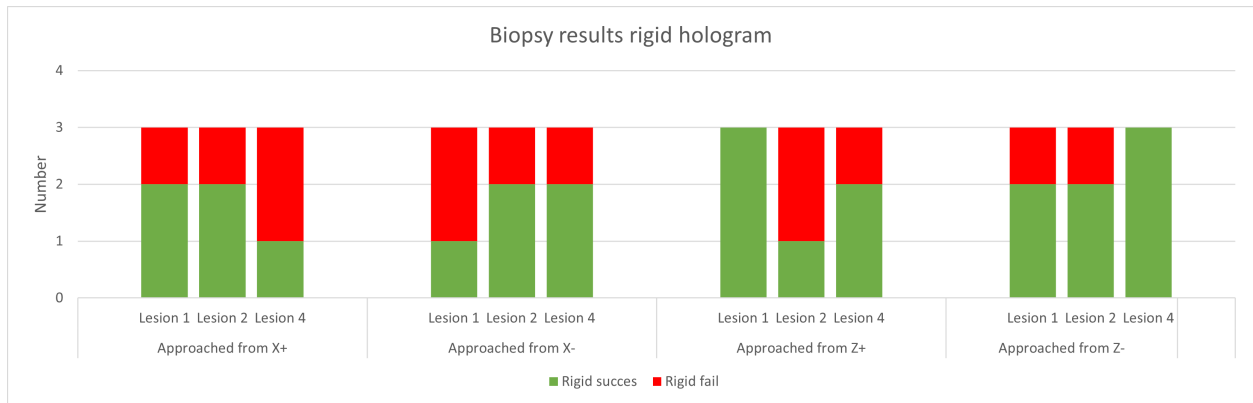


Figure 28: Results of the biopsy experiments with TPS turned off, grouped per direction from which the biopsy is performed.

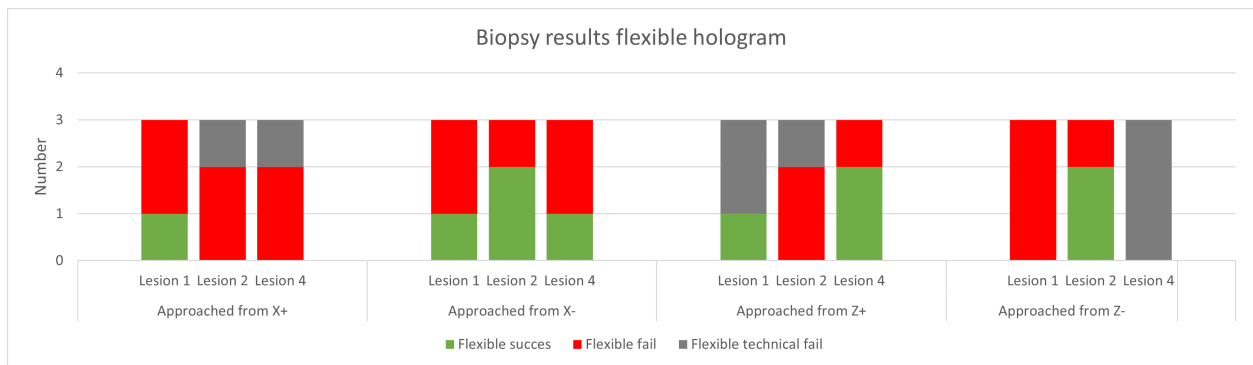


Figure 29: Results of the biopsy experiments with TPS turned on, grouped per direction from which the biopsy is performed.

Each lesion has been targeted 6 times from a certain direction, 3 times with TPS enabled and 3 times with the algorithm disabled. It can be seen that a successful biopsy was much more common when the TPS algorithm was not activate;, 23 times compared to 10 successfully biopsies. The graph also shows that a technical fail occurred 8 times and those fails took place at the X+, Z+ and Z- directions. Combining the outcome of each biopsy results in a success rate of 64% when TPS was disabled and 28% when TPS was enabled. Including the TPS algorithm resulted in a 22% technical fail rate meaning that the biopsy could not be performed due to incorrectness of the solution.

4 Discussion

This chapter will discuss the results that have been shown in chapter 3.

4.1 Hologram placement error evaluation

The first experiment that has been conducted evaluated the error of the hologram placement. Table 4 shows an average error of 8.3 mm. This error is most likely a summation of the individual errors in the pipeline. The markers grouped as the phantom object in the Optitrack system have a mean position error of 1.3mm per marker.

Another source of error is the position of the origin of the homogeneous matrix. When the TPS algorithm is activated, the position of the phantom mesh is calculated according to the location of the markers. When the algorithm is not activated, the mesh is placed using the location of the origin of the PhantomOptitrack coordinate frame, which is received from the Optitrack system. This system creates the origin of a coordinate frame at the center of a group of markers that are all assigned to the same trackable object. This method differs from the way the coordinate frame origin, created by the MRI, is placed. This coordinate frame is positioned in the middle of the scanned object, i.e. the phantom. Since the origin is placed in the middle of the scanned volume, the origin will be positioned below each of the selected phantom markers which are all located at the top of the phantom. This change is also shown in figure 30. The green dots represent the markers. The error in the x and z direction is close to 0 but the error in the height is significant at about 20 mm. This can be observed when looking at the position of the markers; the markers surrounding the blue mesh are all transformed downwards compared to the markers surrounding the red mesh. Further research should add a piece of software that will (i) calculate the center point of the markers, (ii) compare that to the position of the origin of the MRI-scan, and (iii) calculate the homogeneous matrix to link both coordinate frames to eliminate this error.

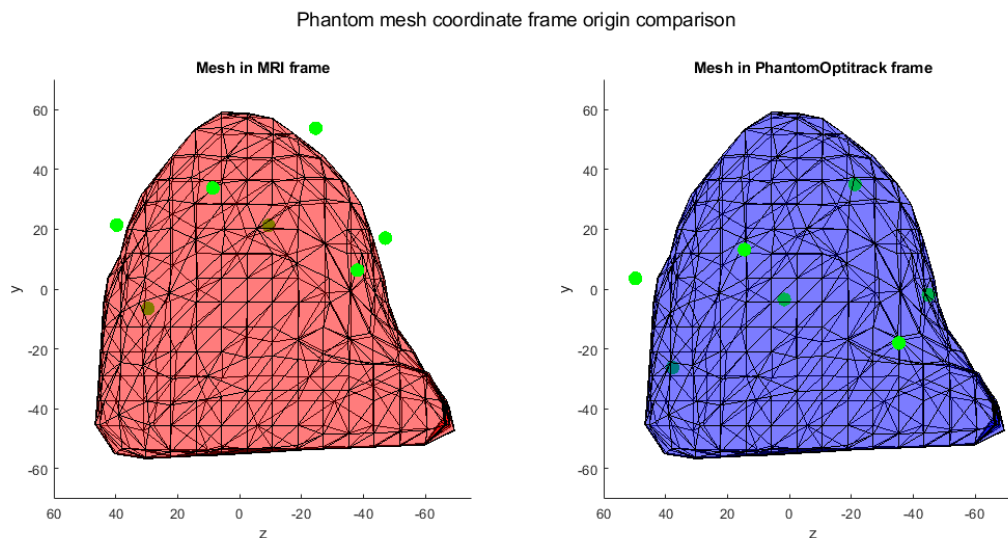


Figure 30: The phantom mesh being projected in the MRI and PhantomOptitrack frame, the markers are given in green. The right figure shows that the origin of the coordinate frame is positioned at the center of all markers while the left figure shows that the origin of the coordinate frame is positioned at the center of the phantom mesh, most markers are positioned above the origin.

The final part of the error is due to inaccuracies in hologram placement of the HoloLens, since the placement of the hologram will never be perfectly stable and at the right position. The holograms sometimes encountered some sort of drift when being visualized on the HoloLens. This would occur when the user was moving around the room a lot and made sudden fast movements. The HoloLens tried to predict the orientation of the HMD in the room but found out, after rescanning the room, that it was actually off. When accounting for this error, the hologram would shift around a bit. This is the reason why one of the x-alignment errors had a value of 15 mm instead of being close to the average error of 5 mm. This drift and misalignment has

also been investigated in other research. Vassallo et al. [40], for instance, found an average placement error of 6 mm when looking at errors placing holograms without markers, which is essentially what is done in this work. The marker positions are not known by the HoloLens, so it only uses its spatial awareness to place a hologram at a certain position in 3D space. Meulstee et al. [28] measured a mean error of 2.3 mm when placing holograms using the same technique as was done in this work. Main differences were that this error was measured in a static setting, only using a single camera and with the camera being much closer to the setup than was the case in this work, reducing the error of the marker positions significantly.

The figure with the manual offset enabled still shows little distortion. This could be explained by inaccuracies that will occur when walking around the hologram. The margins are very small and the HoloLens also generates placement errors of a few millimeters as described above. The hologram seemed to be at a better position when it was displayed on the HoloLens, but by taking the photograph its perspective changed a bit. This is a very difficult and common problem when working with MxR, since the content is only visible for the person wearing the HMD. Whenever a picture is taken, the 3D holograms have to be captured in 2d and the absence of the 3D information will give a different view of the scene than the user experienced at the time the picture was taken.

4.2 Marker filtering

The results of the filtering algorithm, as shown in figure 22, show that this procedure seems to work as intended. The implementation of an ellipsoidal filtering region compared to a spherical one resulted in extra faulty markers being occluded from the matching algorithms, decreasing the risk of a mismatch. The radiuses of the ellipsoid could be optimized to exclude even more markers, but one of the sources of the infrared noise is located within a very small reach of the origin of the frame, located just 30 mm in -Y direction. This factor combined with the current resolution of the Optitrack camera's will quickly result in the occlusion of markers which actually belong to the HoloLens bracket.

The current filter region has its origin positioned at the pivot point of one of the HoloLens markers, as is shown in figure 5. This origin could potentially be moved to be positioned at the center of all markers, as is done with the phantom filter region, to narrow down the x-range of the ellipsoid. Whenever the filter region origin is changed, the y-range does have to be increased to ensure all relevant markers are within the filter region. It should be evaluated which changes to the shape and origin of the filter region will have a noticeable impact on the outcome of the filter step.

4.3 Thin Plate Spline (TPS)

The current implementation of the TPS still suffers from some imperfections. The solution only places the hologram once and afterwards only changes the shape of the mesh and not its position. This is done due to the large shifts of the WorldHoloLens frame, to which these transformations should be mapped. During the tests, large changes were encountered which resulted in the hologram error increasing rather than decreasing when the position was updated. This limitation explains the large error which is visible in figure 31.

4.4 Biopsy

Section 2.4.4 described that each lesion would be used to perform biopsy but the results in section 3.4 only show the results of lesions 1,2 & 4. This is due to two reasons, the first being that the third lesion has been dyed with a light green colour which is hard to distinguish from the tissue of the phantom, especially since the author suffers from a strong form of deutan colorblindness. The other 3 lesions have been colored with a blue dye which is much better distinctable. The second reason is that the lesion location data that has been retrieved by [39] does not align for lesion 3 and the actual accurate position of the lesion could not be retrieved and implemented due to time constraints.

Two types of mistakes were noted down as a technical fail. The first type of technical fail was due to warping of the model when including TPS, as is shown in figure 26. This type of technical fail occurred at the directions X+ & Z+. The second type of technical fail was due to great misalignment of the hologram. Figure 31 shows that the hologram with the TPS activated had an offset that was too big when looking at lesion 4 from the Z- direction such that the lesion was not covered at all and the solution could not properly be tested. This is why all attempts of this lesion from this direction resulted in a technical fail.



Figure 31: Hologram with lesion 4 and TPS enabled. The solution has too much offset and does not cover the lesion of interest, thus disabling the ability to perform a biopsy using the solution.

An incidence which had a negative impact on the outcomes of this experiment was that the second lesion of the phantom sometimes encountered a position change whenever a biopsy was being performed. This is most probably due to wear of the phantom and the multiple needle insertions that have been performed on this lesion in this work and by Tichelaar [39]. This resulted in the needle pressing the stiff lesion away instead of perforating it, resulting in the needle being at the correct position but no lesion tissue being extracted. An example of this is shown in figure 32.

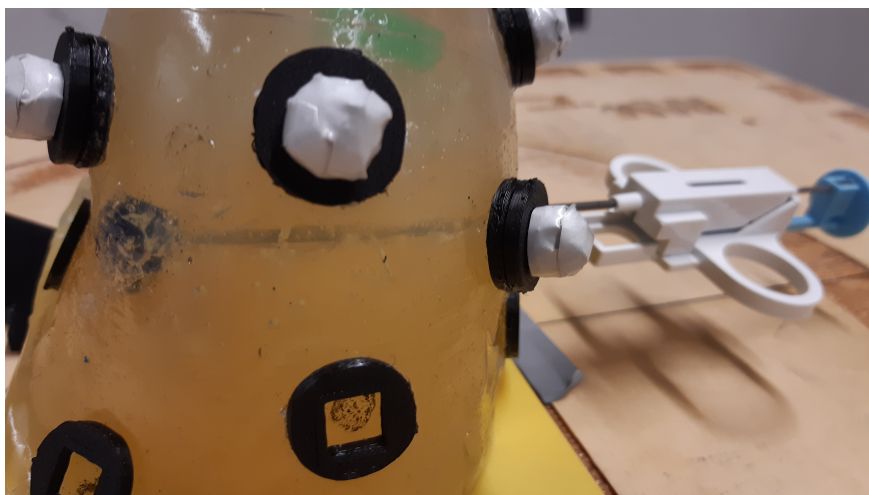


Figure 32: The needle after targeting lesion 2. This attempt was actually a miss while the image makes it believe that the lesion was hit.

Another limitation of the experiment was the lack of updated depth information of the needle. It would have been preferable to have implemented some sort of visual feedback, by means of a needle hologram for instance, that would be rendered to graphically display the distance to the lesion of interest and perhaps also implement a text box with the actual x,y and z distances of the error between the needle tip and the lesion. It would especially help inexperienced operators, like the author, to improve their skills in estimating the position of the needle tip based on the position and orientation of the biopsy gun. This solution would require additional markers on the biopsy gun such that it can be tracked, but this has been done in previous research and it should be possible to implement such a solution in the current implementation [39] [33].

Section 2.4.4 described that the transparency of the hologram would be set to 0.5 to ensure that the inside

of the phantom was not visible. This was the case for lesion one, which is positioned somewhat at the center of the phantom, but this solution did not block the lesions sufficient for lesion two and four. Therefore, the transparency was increased to 1 for these lesions. This made it more difficult to insert the needle correctly, since it was hard to look at the angle and the remaining length of the needle before entering the phantom, and thus hard to estimate whether the lesion was hit or not.

The needle encountered much more resistance from the phantom tissue whenever a lesion had to be targeted that was positioned at the opposite side of the biopsy direction. The friction component was almost neglectable when the lesion was being targeted from the direction which resulted in the shortest distance to the lesion. This can also be seen by combing the locations of the lesions shown in figure 16 and the results shown in figures 28 & 29 , since more successful biopsies were performed when the user was close to the lesion it was targeting. This indicated that being able to walk around the phantom and visually judge which angle and position of insertion was optimal, which was described as a major drawback of the current MRI-guided biopsy systems, resulted in less friction and less misses when performing a biopsy with the current solution.

5 Conclusion & Future work

This project has focused on implementing a solution that could visualize MRI-only visible lesions using MxR and the HoloLens. The solution consists of three components, the first component being the Optitrack camera system that registers the location of trackable markers in 3D space. The second component is the Matlab program that processes this data and creates a hologram which accounts for deformations that might occur during biopsy. The input marker data first gets filtered to exclude markers which are not close to a trackable object. Afterwards the markers get assigned to the correct object by comparing the inter marker distances, angles and heights. Whenever the Thin Plate Spline algorithm is active, deformations of the phantom and lesion positions will be calculated with respect to the marker positions and the mesh data will be updated accordingly. The final component of the implemented solution is the C# program that runs on the HoloLens. This program receives data from the Matlab program using a TCP/IP protocol, creates the holograms and renders them at the correct position in space using the spatial awareness features of the HoloLens.

The first subquestion to be answered is: "How accurate can the virtual model of the breast be projected over the real breast?" The results show that the hologram can be positioned with an error (E) of $(E_x, E_y, E_z) = (7.2, 9.6, 8.1)$ mm. This error is a summation of errors generated by the Optitrack system and the HoloLens. Improving the accuracy of the data created in these components will reduce the error and thus result in more accurately placed holograms.

The second subquestion was: "What is the success rate when biopsy is performed using the Mixed Reality lesion model?" The results show that a successful biopsy was performed in 64% of the cases when TPS was disabled and 28% of the times when TPS was enabled. Including the TPS algorithm resulted in a 15% technical fail rate meaning that the biopsy could not be performed due to incorrectness of the solution. This was either through misalignment or warping of the mesh due to a wrong outcome of the marker matching algorithms. Besides misalignment and warping, the lack of experience of the operator when performing biopsies also had negative impact on the biopsy results and these aspects should be evaluated when improving the current solution.

To conclude this work the main research question will be answered, which is: "How does the success rate of performing biopsy of MRI-only visible lesions in the female breast when using a Mixed reality guidance system and a deformation model compare with current techniques?" The total success rate of the performed biopsies is 46%, these rates are lower than the success rates that are achieved by current techniques which were 100% for the LCNB and 98% for the VAB. [27][20]. Despite the final solution not surpassing the success rate of current techniques, further research in the area of using Mixed Reality for medical purposes could result in promising state-of-the-art products that aim to aid medical specialists in performing biopsies with more accuracy.

5.1 Future work

Some recommendations for future work to further improve the proposed solution will be given below.

Despite this research showing promising biopsy results, a limitation on the results of the biopsy experiment is the absence of 3D needle data to be able to evaluate the needle placement error. A 3D position measurement setup, like the Aurora NDI electromagnetic tracking system (Northern Digital, Waterloo, Canada), could be used to evaluate the needle placement error and acquire even more insights regarding the direction and magnitude of the error instead of just registering whether the lesion was hit or missed.

The software that combines the data from the Optitrack camera's, Tracking tools, is quite dated. The new variant of the software, Motive (NaturalPoint, Inc., Corvallis, OR, USA), packs some extra features like the linking of measured marker data to a certain object, which would be very useful for this project. The marker processing algorithms would only have to correctly map markers within an object and the filtering step could be removed, since the markers would already be assigned to either the HoloLens or the phantom.

Microsoft has created a newer version of the HoloLens, called the HoloLens 2, which has updated features like eye tracking, a wider FoV, tracking of both hands, upgraded hardware like the CPU & RAM and is capable of displaying higher resolution holograms. This might help with the current misalignment problem which has been described in sections 3.1 & 4.1 and improve the overall MxR experience.

The current cameras used in the Optitrack system have a resolution of 640 x 480 pixels. Newer versions of the Optitrack camera's can recorded up to 2048 x 2048 pixels with a frame rate of 180 Hz which will

increase the accuracy of the marker positions and thus also improve the precision with which a hologram can be placed in the work space of the camera's.

If higher resolution camera's can be implemented more markers could be positioned on the phantom since there would be less overlap between individual markers. This would improve the accuracy with which deformations could be tracked, since the TPS algorithm could track the deformation using more reference points. A downside could be that the markers which are currently used might not be round enough to take advantage of the roundness filter function of the tracking software. In that case, the markers could be replaced with a commercially available solution, with the side note that the markers need to be visible in both the MRI scanner and the Optitrack system.

The Thin Plate Spline algorithm shows promising results for accurately tracking deformations of a phantom, but additional research has to be conducted to see to what extent the method can describe deformations of actual female breasts, since each breast is different and will react differently to the insertion of a needle. Female breasts are mostly less stiff than the phantom used in this work and the work of Lagomarsino [24] so it should be evaluated whether TPS still gives accurate results when used to track lesions in real breasts.

The current software has been created as a proof of concept, additional work has to be done before the solution can be used in an actual hospital. Since patient data is used, data encryption is a very important aspect which has not been implemented in the current implementation. The software could also be implemented in C++ instead of Matlab to further optimize the time it takes to complete a full loop and take advantage of all features this programming language has to offer.

6 Appendix A: Homogeneous matrices

6.1 Overview of frames

The coordinate frames that have been used in this work are described below. Each frame has been given a name such that it is easy to distinguish whether the coordinate frame is used to describe data being used by the HoloLens (HoloLens) or the Optitrack system (Optitrack).

- WorldOptitrack
- WorldHoloLensMeterLeft
- WorldHoloLens
- HoloLensPivotOptitrack
- HoloLensCameraOptitrack
- HoloLensCameraHoloLensMeterLeft
- HoloLensCameraHoloLens
- PhantomOptitrack

6.2 Static transformations

Some of the homogeneous transformation matrices are known up front since the transformation between two frames is static, these matrices are described below:

$$H_{\text{MeterLeft}}^{\text{MillimeterRight}} = \begin{bmatrix} 1000 & 0 & 0 & 0 \\ 0 & 1000 & 0 & 0 \\ 0 & 0 & -1000 & 0 \\ 0 & 0 & 0 & 1 \end{bmatrix} \quad (7)$$

$$H_{\text{HoloLensCameraOptitrack}}^{\text{HoloLensCameraHoloLens}} = \begin{bmatrix} 1 & 0 & 0 & 0 \\ 0 & 1 & 0 & 0 \\ 0 & 0 & 1 & 0 \\ 0 & 0 & 0 & 1 \end{bmatrix} \quad (8)$$

$$H_{\text{HoloLensPivotOptitrack}}^{\text{HoloLensCameraOptitrack}} = \begin{bmatrix} 1 & 0 & 0 & 28 \\ 0 & 1 & 0 & 46 \\ 0 & 0 & 1 & 8 \\ 0 & 0 & 0 & 1 \end{bmatrix} \quad (9)$$

The values shown in equation 9 have been measured by hand so measurement errors of 1-2mm could be present in the transformation part of this homogeneous matrix. All the transformation matrices that have not been described in this section are measured by either the Optitrack system or the HoloLens and their values will change each iteration of the program.

6.3 Chained multiplications

Since all of the transformation matrices which are retrieved from the HoloLens are in a left handed coordinate frame and in meters, they will first be transformed to be described in the right handed coordinate frame and in millimeters. Whenever such matrix is transformed to hold this configuration the subscript MillimeterRight is dropped. The multiplication that has been done to transform the MeterLeft matrix is shown in equation 10.

$$H_{\text{HoloLensCameraHoloLens}}^{\text{WorldHoloLens}} = H_{\text{MeterLeft}}^{\text{MillimeterRight}} H_{\text{HoloLensCameraHoloLensMeterLeft}}^{\text{WorldHoloLensMeterLeft}} \text{inv}(H_{\text{MeterLeft}}^{\text{MillimeterRight}}) \quad (10)$$

In order to correctly project the hologram of the phantom relevant to the HoloLens, $H_{\text{PhantomOptitrack}}^{\text{WorldHoloLens}}$ has to be calculated. The result is shown in equation 11.

$$H_{\text{PhantomOptitrack}}^{\text{WorldHoloLens}} = H_{\text{HoloLensCameraHoloLens}}^{\text{WorldHoloLens}} H_{\text{HoloLensCameraOptitrack}}^{\text{HoloLensCameraHoloLens}} H_{\text{HoloLensPivotOptitrack}}^{\text{HoloLensCameraOptitrack}} H_{\text{WorldOptitrack}}^{\text{HoloLensPivotOptitrack}} H_{\text{PhantomOptitrack}}^{\text{WorldOptitrack}} \quad (11)$$

This matrix will be transformed to use meters and the left handed coordinate frame by performing the transformation shown in equation 12.

$$H_{\text{WorldHoloLensMeterLeft}}^{\text{PhantomOptitrackMeterLeft}} = \text{inv}(H_{\text{MeterLeft}}^{\text{MillimeterRight}}) H_{\text{WorldHoloLensMeterLeft}}^{\text{PhantomOptitrackMeterLeft}} H_{\text{MeterLeft}}^{\text{MillimeterRight}} \quad (12)$$

References

- [1] ArUco: a minimal library for Augmented Reality applications based on OpenCV — Aplicaciones de la Visión Artificial. URL <http://www.uco.es/investiga/grupos/ava/node/26>.
- [2] HoloLens (1st gen) hardware — Microsoft Docs. URL <https://docs.microsoft.com/en-us/hololens/hololens1-hardware>.
- [3] GitHub - microsoft/MixedRealityToolkit-Unity: Mixed Reality Toolkit (MRTK) provides a set of components and features to accelerate cross-platform MR app development in Unity. URL <https://github.com/microsoft/MixedRealityToolkit-Unity>.
- [4] What's Inside Microsoft's HoloLens And How It Works — Tom's Hardware. URL <https://www.tomshardware.com/news/microsoft-hololens-components-hpu-28nm,32546.html>.
- [5] U.S. Breast Cancer Statistics — Breastcancer.org. URL https://www.breastcancer.org/symptoms/understand{_}bc/statistics.
- [6] Unity Real-Time Development Platform — 3D, 2D VR & AR Engine. URL <https://unity.com/>.
- [7] Cleveland Clinic Using Augmented Reality to Enhance Liver Cancer Therapy – Cleveland Clinic Newsroom. URL <https://newsroom.clevelandclinic.org/2019/01/14/cleveland-clinic-using-augmented-reality-to-enhance-liver-cancer-therapy/>.
- [8] Briton Bauerly - HoloStand stand for Microsoft HoloLens. URL <https://www.thingiverse.com/thing:1723390>.
- [9] Calibration Squares - NaturalPoint Product Documentation Ver 2.2. URL https://v22.wiki.optitrack.com/index.php?title=Calibration_Squares.
- [10] Breast Magnetic Resonance Imaging (MRI) — Johns Hopkins Medicine. URL <https://www.hopkinsmedicine.org/health/treatment-tests-and-therapies/breast-mri>.
- [11] Survival Rates for Breast Cancer. URL <https://www.cancer.org/cancer/breast-cancer/understanding-a-breast-cancer-diagnosis/breast-cancer-survival-rates.html>.
- [12] ECMA-334 5 th Edition / C# Language Specification. Technical report, 2017. URL www.ecma-international.org.
- [13] Patric Bettati, Majid Chalian, James Huang, James D. Dormer, Maysam Shahedi, and Baowei Fei. Augmented reality-assisted biopsy of soft tissue lesions. (March 2020):31, 2020. ISSN 0277-786X. doi: 10.1117/12.2549381.
- [14] Carla Boetes and Ritse M. Mann. Ductal carcinoma in situ and breast MRI. *The Lancet*, 370(9586): 459–460, aug 2007. ISSN 0140-6736. doi: 10.1016/S0140-6736(07)61207-0.
- [15] Carol E. DeSantis, Jiemin Ma, Mia M. Gaudet, Lisa A. Newman, Kimberly D. Miller, Ann Goding Sauer, Ahmedin Jemal, and Rebecca L. Siegel. Breast cancer statistics, 2019. *CA: A Cancer Journal for Clinicians*, 69(6):438–451, 2019. ISSN 0007-9235. doi: 10.3322/caac.21583.
- [16] Mathieu Garon, Pierre Olivier Boulet, Jean Philippe Doironz, Luc Beaulieu, and Jean Francois Lalonde. Real-Time High Resolution 3D Data on the HoloLens. *Adjunct Proceedings of the 2016 IEEE International Symposium on Mixed and Augmented Reality, ISMAR-Adjunct 2016*, pages 189–191, 2017. doi: 10.1109/ISMAR-Adjunct.2016.0073.
- [17] Vincent Groenhuis, Françoise J Siepel, and Stefano Stramigioli. G 22 Sunram 5: A Magnetic Resonance-Safe Robotic System for Breast Biopsy, Driven by Pneumatic Stepper Motors. 2020. doi: 10.1016/B978-0-12-814245-5.00022-0. URL <https://doi.org/10.1016/B978-0-12-814245-5.00022-0>.
- [18] Judith M. Hemmer, Johannes C. Kelder, and Hans P.M. van Heesewijk. Stereotactic large-core needle breast biopsy: Analysis of pain and discomfort related to the biopsy procedure. *European Radiology*, 18(2):351–354, feb 2008. ISSN 09387994. doi: 10.1007/s00330-007-0762-3. URL <https://pubmed.ncbi.nlm.nih.gov/17007623/>.
- [19] D. I. Hoult and B. Bhakar. NMR signal reception: Virtual photons and coherent spontaneous emission. *Concepts in Magnetic Resonance*, 9(5):277–297, 1997. ISSN 10437347. doi: 10.1002/(sici)1099-0534(1997)9:5<277::aid-cmr1>3.0.co;2-w.

- [20] Thomas Imschweiler, Harald Haueisen, Gert Kampmann, Luzi Rageth, Burkhardt Seifert, Christoph Rageth, Bianka Freiwald, and Rahel A Kubik-Huch. MRI-guided vacuum-assisted breast biopsy: comparison with stereotactically guided and ultrasound-guided techniques. doi: 10.1007/s00330-013-2989-5. URL www.mibb.ch.
- [21] J. L. Jiménez Bascones, Manuel Graña, and J. M. Lopez-Guede. Robust labeling of human motion markers in the presence of occlusions. *Neurocomputing*, 353:96–105, aug 2019. ISSN 18728286. doi: 10.1016/j.neucom.2018.05.132.
- [22] Bernard C. Kress and William J. Cummings. Optical architecture of HoloLens mixed reality headset. *Digital Optical Technologies 2017*, 10335(June 2017):103350K, 2017. ISSN 1996756X. doi: 10.1117/12.2270017.
- [23] Christian Kunz, Paulina Maurer, Fabian Kees, Pit Henrich, Christian Marzi, Michal Hlaváč, Max Schneider, and Franziska Mathis-Ullrich. Infrared marker tracking with the HoloLens for neurosurgical interventions. *Current Directions in Biomedical Engineering*, 6(1):1–4, 2020. ISSN 23645504. doi: 10.1515/cdbme-2020-0027.
- [24] Martha Lagomarsino. *Deformation tracking and compensation in image-guided breast biopsy with hand-mounted motorized needle angulation tool*. Master thesis dissertation, University of Genova, 2020.
- [25] D. Leithner, G. J. Wengert, T. H. Helbich, S. Thakur, R. E. Ochoa-Albiztegui, E. A. Morris, and K. Pinker. Clinical role of breast MRI now and going forward. *Clinical Radiology*, 73(8):700–714, 2018. ISSN 1365229X. doi: 10.1016/j.crad.2017.10.021. URL <https://doi.org/10.1016/j.crad.2017.10.021>.
- [26] Yang Liu, Haiwei Dong, Longyu Zhang, and Abdulmotaleb El Saddik. Technical evaluation of HoloLens for multimedia: A first look. *IEEE Multimedia*, 25(4):8–18, 2018. ISSN 19410166. doi: 10.1109/MMUL.2018.2873473.
- [27] Carla Meeuwis, Jeroen Veltman, Hester N. Van Hall, Roel D.M. Mus, Carla Boetes, Jelle O. Barentsz, and Ritse M. Mann. MR-guided breast biopsy at 3T: Diagnostic yield of large core needle biopsy compared with vacuum-assisted biopsy. *European Radiology*, 22(2):341–349, 2012. ISSN 09387994. doi: 10.1007/s00330-011-2272-6.
- [28] Jene W. Meulstee, Johan Nijsink, Ruud Schreurs, Luc M. Verhamme, Tong Xi, Hans H.K. Delye, Wilfred A. Borstlap, and Thomas J.J. Maal. Toward Holographic-Guided Surgery. *Surgical Innovation*, 26(1):86–94, 2019. ISSN 15533514. doi: 10.1177/1553350618799552.
- [29] Paul Milgram. A TAXONOMY OF MIXED REALITY VISUAL DISPLAYS. Technical Report 12, 1994. URL http://vered.rose.utoronto.ca/people/paul/{_}dir/IEICE94/ieice.html.
- [30] Amanda Norberg, Amanda Norberg, and Elliot Rask. *3D visualisation of breast reconstruction using Microsoft HoloLens*. Master thesis, Uppsala University, 2018.
- [31] Brian J. Park, Stephen J. Hunt, Gregory J. Nadolski, and Terence P. Gade. Augmented reality improves procedural efficiency and reduces radiation dose for CT-guided lesion targeting: a phantom study using HoloLens 2. *Scientific Reports*, 10(1):1–8, 2020. ISSN 20452322. doi: 10.1038/s41598-020-75676-4. URL <https://doi.org/10.1038/s41598-020-75676-4>.
- [32] Stephanie L. Perkins, Michael A. Lin, Subashini Srinivasan, Amanda J. Wheeler, Brian A. Hargreaves, and Bruce L. Daniel. A Mixed-Reality System for Breast Surgical Planning. *Adjunct Proceedings of the 2017 IEEE International Symposium on Mixed and Augmented Reality, ISMAR-Adjunct 2017*, pages 269–274, 2017. doi: 10.1109/ISMAR-Adjunct.2017.92.
- [33] Long Qian, Anton Deguet, Zerui Wang, Yun Hui Liu, and Peter Kazanzides. Augmented reality assisted instrument insertion and tool manipulation for the first assistant in robotic surgery. In *Proceedings - IEEE International Conference on Robotics and Automation*, volume 2019-May, pages 5173–5179. Institute of Electrical and Electronics Engineers Inc., may 2019. ISBN 9781538660263. doi: 10.1109/ICRA.2019.8794263.
- [34] K Rohr, H S Stiehl, R Sprengel, W Beil, T M Buzug, J Weese, and M H Kuhn. Point-Based Elastic Registration of Medical Image Data Using Approximating Thin-Plate Splines. Technical report.
- [35] Somaieh Rokhsaritalemi, Abolghasem Sadeghi-Niaraki, and Soo Mi Choi. A review on mixed reality: Current trends, challenges and prospects. *Applied Sciences (Switzerland)*, 10(2), 2020. ISSN 20763417. doi: 10.3390/app10020636.

- [36] Gerd Schueller, C. Schueller-Weidekamm, and T. H. Helbich. Accuracy of ultrasound-guided, large-core needle breast biopsy. *European Radiology*, 18(9):1761–1773, 2008. ISSN 09387994. doi: 10.1007/s00330-008-0955-4. URL <https://pubmed.ncbi.nlm.nih.gov/18414872/>.
- [37] Toby Sharp, Cem Keskin, Duncan Robertson, Jonathan Taylor, Jamie Shotton, David Kim, Christoph Rhemann, Ido Leichter, Alon Vinnikov, Yichen Wei, Daniel Freedman, Pushmeet Kohli, Eyal Krupka, Andrew Fitzgibbon, and Shahram Izadi. Accurate, robust, and flexible realtime hand tracking. *Conference on Human Factors in Computing Systems - Proceedings*, 2015-April:3633–3642, 2015. doi: 10.1145/2702123.2702179.
- [38] Oren M. Tepper, Hayeem L. Rudy, Aaron Lefkowitz, Katie A. Weimer, Shelby M. Marks, Carrie S. Stern, and Evan S. Garfein. Mixed reality with hololens: Where virtual reality meets augmented reality in the operating room. *Plastic and Reconstructive Surgery*, 140(5):1066–1070, 2017. ISSN 00321052. doi: 10.1097/PRS.0000000000003802.
- [39] Jos Tichelaar. *Tracking and compensation for breast deformations during image-guided breast biopsy with a hand-mounted biopsy tool*. Master thesis dissertation, University of Twente, Enschede, 2021.
- [40] Reid Vassallo, Adam Rankin, Elvis C. S. Chen, and Terry M. Peters. Hologram stability evaluation for Microsoft HoloLens. *Medical Imaging 2017: Image Perception, Observer Performance, and Technology Assessment*, 10136(March 2017):1013614, 2017. ISSN 16057422. doi: 10.1117/12.2255831.
- [41] Jose D. Velazco-Garcia, Dipan J. Shah, Ernst L. Leiss, and Nikolaos V. Tsekos. A modular and scalable computational framework for interactive immersion into imaging data with a holographic augmented reality interface. *Computer Methods and Programs in Biomedicine*, 198:105779, 2021. ISSN 18727565. doi: 10.1016/j.cmpb.2020.105779. URL <https://doi.org/10.1016/j.cmpb.2020.105779>.
- [42] Anne M. Wallace, Christopher Comstock, Carl K. Hoh, and David R. Vera. Breast imaging: A surgeon’s prospective. *Nuclear Medicine and Biology*, 32(7):781–792, 2005. ISSN 09698051. doi: 10.1016/j.nucmedbio.2005.07.008.